RESOURCES *for the* FUTURE

Uncertain Remedies to Fight Uncertain Consequences: The Case of Solar Geoengineering

Felix D. Meier and Christian P. Traeger

Working Paper 23-37
September 2023

About the Authors

Felix D. Meier works in the Global Commons and Climate Policy research center in the Institute for the World Economy at Kiel University. He obtained his doctorate in economics from Kiel University. His primary research interests are the recent shale gas boom in the US and the economic potential of climate engineering technologies in regional integrated assessment models.

Christian P. Traeger is a professor in the Department of Economics at the University of Oslo and research director at the ifo Center for Energy, Climate, and Resources.

About the Project

The Resources for the Future Solar Geoengineering research project applies tools from multiple social science research disciplines to better understand the risks, potential benefits, and societal implications of solar geoengineering as a possible approach to help reduce climate risk alongside aggressive and necessary mitigation and adaptation efforts. The project began in 2020 with a series of expert workshops convened under the SRM Trans-Atlantic Dialogue. These meetings resulted in a 2021 article in Science that lays out a set of key social science research questions associated with solar geoengineering research and potential deployment. The Project followed this with additional sponsored research, including a competitive solicitation designed to address research areas highlighted in the Science article. This paper is one of eight research papers resulting from that competition and supported by two author workshops. A key goal of the solicitation and the overall project is to engage with a broader set of researchers from around the globe, a growing number of interested stakeholders, and the public.

Acknowledgements

We acknowledge support from the LAD Climate Fund and useful comments and feedback from workshops at Resources for the Future. We are particularly grateful for feedback from Mariia Belaia, Simon Dietz, Moritz Drupp, Hermann Held, Juan Moreno-Cruz, Grischa Perino, Billy Pizer, Rick van der Ploeg, Martin Quaas, Wilfried Rickels, Frank Venmans, and Daniele Visioni.

About RFF

Resources for the Future (RFF) is an independent, nonprofit research institution in Washington, DC. Its mission is to improve environmental, energy, and natural resource decisions through impartial economic research and policy engagement. RFF is committed to being the most widely trusted source of research insights and policy solutions leading to a healthy environment and a thriving economy.

Working papers are research materials circulated by their authors for purposes of information and discussion. They have not necessarily undergone formal peer review. The views expressed here are those of the individual authors and may differ from those of other RFF experts, its officers, or its directors.

Sharing Our Work

Uncertain Remedies to Fight Uncertain Consequences: The Case of Solar Geoengineering

Felix D. Meier[#] and Christian P. Traeger[*]

November 14, 2022

Abstract

Solar geoengineering can cool our planet and counteract the warming caused by greenhouse gas emissions. Given current emission trajectories, solar geoengineering has the potential to save lives, reduce severe impacts on economic production, and save ecosystems and island states. Deterministic integrated assessment models tend to show major benefits from solar geoengineering, but are highly sensitive to the assumed and highly uncertain damages from solar geoengineering as well as the effectiveness of cooling the planet. We analyze how uncertainties and the anticipation of learning change the case for solar geoengineering in a world with an uncertain temperature response to carbon dioxide emissions.

JEL Codes: Q54, H23, H43, E13, D80, D61

Keywords: geoengineering, climate change, integrated assessment, uncertainty, learning, social cost of carbon

[#]Kiel Institute for the World Economy (felix.meier@ifw-kiel.de). [*]Department of Economics, University of Oslo (traeger@uio.no); CESifo Munich. We acknowledge support from the L.A.D. Climate Fund and useful comments and feedback from workshops at Resources for the Future. We are particularly grateful for feedback from Mariia Belaia, Simon Dietz, Moritz Drupp, Hermann Held, Juan Moreno-Cruz, Grischa Perino, Billy Pizer, Rick van der Ploeg, Martin Quaas, Wilfried Rickels, Frank Venmans, and Daniele Visioni.

1 Introduction

Sulfur-based geoengineering offers an affordable measure to counter dangerous climate change at the global scale. However, the potential remedy is accompanied by novel risks and uncertainties. These risks involve immediate and long-term damages from the employed cooling agent as well as solar geoengineering itself. Possible impacts are changes in precipitation, acid rain, depletion of the ozone layer, and direct impacts on crop-yields caused by changes of the incoming light (Crutzen 2006, Heckendorn et al. 2009, Keith and MacMartin 2015). These potential impacts are highly uncertain, and it is unlikely that these uncertainties can be reduced substantially before testing solar geoengineering on a large scale. Many studies suggest that solar geoengineering is a highly cost effective tool to counter geoengineering when relying on expected efficiency and best guess damages. At the same time, many scientists have been warning of the dangers of even investigating the option of solar geoengineering because it could counter mitigation efforts, e.g., Biermann et al. (2022) prominently urge for an international non-use agreement on solar geoengineering.

The present paper analyzes how uncertainties with and without the anticipation of learning change the rationale of undertaking geoengineering. We explicitly introduce uncertainty over the damages from sulfur-based geoengineering and its cooling efficiency into an integrated assessment model of climate change and solar geoengineering. We distinguish between persistent long-run uncertainty and quickly resolving short-term uncertainty. The quickly resolving short-term uncertainty allows the policy maker to actively learn from large scale deployment. Such learning only impacts the initial deployment decision when a policy maker foresees the learning and anticipates how future use of geoengineering can be conditioned on the realized damages and cooling efficiency. We solve for the rational deployment strategies before and after learning. We also evaluate these deployment strategies from the perspective of policy makers who merely pay attention to the immediate expected net benefits of deployment. We also formalize the concern that the execution of and learning about sulfur-based geoengineering can reduce the incentive to mitigate greenhouse gas emissions. The incentive to reduce emission is captured in the social cost of carbon (SCC). We show how uncertainty, the anticipation of learning, and having learned affects the incentive to mitigate.

Our model delivers both analytic and quantitative results. We provide explicit formulas for optimal geoengineering deployment as well as the SCC. For this purpose, we rely on Meier and Traeger's (2022) SolACE model introducing solar geoengineering into

Traeger's (2021) Analytic Climate Economy model (ACE). The model combines a careful calibration of sulfur's nonlinear forcing contributions and climate dynamics with a general economic production system. To integrate uncertainty, we rely on and extend approaches from Traeger (2018). Following Epstein and Zin (1991), we separate risk aversion from the intertemporal elasticity of substitution – which we assume to be unity as in Tallarini Jr (2000). As a result, we can introduce reasonable levels of risk aversion without unduly discounting the future, addressing concerns raised in the risk-premium and risk-free rate puzzles.

Literature. Our contribution connects the literature on solar geoengineering with the literature on stochastic integrated assessment of climate change. Many authors find that optimally deployed solar geoengineering can reduce climate damages (Nordhaus and Boyer 2000, Moreno-Cruz et al. 2012, Bahn et al. 2015) and we refer to Harding and Moreno-Cruz (2016), Heutel et al. (2016) and Flegal et al. (2019) for a more comprehensive discussion of this literature. Solar geoengineering introduces several new uncertainties to integrated assessment models of climate change, including uncertainties governing geoengineering damages and the radiative forcing response to stratospheric sulfur injections (Heutel et al. 2018). Goes et al. (2011b) analyze the sensitivity to and robustness of geoengineering strategies under a wide set of scenarios. Heutel et al. (2018) find that uncertainty about the climate's sensitivity increases geoengineering whereas uncertainty over the damages of geoengineering reduces the optimal deployment. Heutel et al. (2016) find that solar geoengineering is effective in dealing with tipping points that affect the responsiveness of temperature to carbon, but less effective in dealing with tipping points leading to direct economic losses. Emmerling and Tavoni (2018a) analyze the impact of an uncertain future implementation of geoengineering on present emissions in a two period model of climate change and Kelly et al. (2021) show that sulfur-based geoengineering slows down the learning of the climate sensitivity in a stochastic extension of the DICE model. Helwegen et al. (2019) investigate solar geoengineering deployment in a stochastic version of the DICE model. Roshan et al. (2019) use cost-risk analysis to evaluate the optimal mix of solar geoengineering and mitigation under probabilistic information about climate sensitivity. Manoussi and Xepapadeas (2017) develop a dynamic solar geoengineering game, extended to a setting of uncertainty and robust control in Manoussi et al. (2018).

We connect this literature to a recent literature on analytic approaches to the integrated assessment of climate change. Golosov et al. (2014) and Gerlagh and Liski (2018) deliver a break-through in analytic integrated assessment modeling, and Traeger (2021)

develops the approach to a full-fledged integrated assessment model with state of the art climate dynamics and a general set of energy sectors. We build on Meier and Traeger's (2022) extension of the model integrating solar geoengineering and ocean acidification. Our model advances the two literatures by delivering a new quantitative assessment of the costs and benefits of solar geoengineering under uncertainty. Thereby, we connect to early semi-analytic approaches to climate change assessment under uncertainty Hoel and Karp (2001), Newell and Pizer (2003), Karp and Zhang (2006) as well as more recent approaches employing full-fledged integrated assessment models Traeger (2018), Van den Bremer and Van der Ploeg (2021).

2 The SolACE Model

This section briefly summarizes the deterministic SolACE model developed in Meier and Traeger (2022). The model introduces the option of sulfur-based Solar geoengineering into Traeger's (2021) Analytic Climate Economy (ACE) model. We review the main equations and results under certainty.

2.1 Major model components

Economic Production. Final output is a function of capital, labor, fossil energy, renewable energy, and the technology levels in different sectors. We write gross world output as

$$Y_t = \mathcal{F}(\boldsymbol{A}_t, \boldsymbol{K}_t, \boldsymbol{N}_t, \boldsymbol{E}_t) \tag{1}$$

where the vector $\boldsymbol{A}_t$ characterizes the exogenously evolving technology levels, the vectors $\boldsymbol{K}_t$ and $\boldsymbol{N}_t$ optimally distributed capital and labor across sectors, and $\boldsymbol{E}_t$ a vector of energy inputs. Our only assumption on the production function is homogeneity of degree $\kappa \in (0, 1)$ in capital, a setting that includes the Cobb-Douglas final production with a CES energy sector of Golosov et al. (2014), the DICE setting of Nordhaus and Sztorc (2013), as well as a more general setting with several final goods of varying energy intensity and distinct substitutabilities between fossil and renewable energy sources Traeger (2022). Fossil fuel resources can be scarce, in which case their Hotelling rent interacts with the social cost of carbon incentivizing mitigation.

Climate. CO_2 emissions accumulate in the atmosphere and other carbon sinks following a classical carbon cycle model. It is convenient to measure the resulting atmospheric CO_2 concentration $M_{1,t}$ relative to the preindustrial concentration as $m_t = \frac{M_{1,t}}{M_{\text{pre}}}$. Atmospheric CO_2 causes a greenhouse effect that increases atmospheric temperatures, which we model using Traeger's (2021) non-linear atmosphere-ocean temperature dynamic system. The resulting global atmospheric temperature $T_{1,t}$ measures the increase over 1900 in degree Celsius. In scientific terms, the strength of the greenhouse effect and of sulfur-based cooling are measured in terms of their radiative forcing, which characterizes the energy flux warming or cooling our planet. To cool our planet, we can deploy sulfur S_t (in the form of sulfur dioxide) into our stratosphere, i.e., our atmosphere above the clouds. The SolACE model characterizes the resulting radiative forcing as

$$F_t(m_t, S_t) = \frac{\eta}{\log(2)} \log \left(\underbrace{f_0 + f_1\, m_t + \left(f_2 - f_3 \left(\frac{m_t}{S_t} \right)^n \right) S_t}_{\equiv\, F_t^{CO2}} \right). \tag{2}$$

The expression F_t^{CO2} characterizes the joint radiative forcing of CO_2 and sulfur in CO_2 equivalents. In the absence of solar geoengineering , only the second term in F_t^{CO2} would contribute. The inner bracket relying on the parameters f_2 and f_3 reduces the forcing in response to sulfur injections S_t. The main contribution derives from the term $f_3 \left(\frac{m_t}{S_t} \right)^n$, multiplying the stratospheric sulfur. Sulfur forcing is more efficient relative to CO_2 the larger the atmospheric carbon concentration and the lower the sulfur concentration. At high injection rates, sulfur particles lump together decreasing their cooling efficiency. As a result, scientists expect an asymptotic limit for the cooling from stratospheric aerosol injections (Lawrence et al. 2018). The higher the CO_2 concentration, the lower the warming implied by the marginal ton of CO_2 and the higher the relative forcing reduction of sulfur, which we measure in CO_2 equivalents. We summarize both of these nonlinearities in the joint term whose level effect is captured by f_3 and whose nonlinearity is captured by $n > 0$.

Damages. Temperature increase, carbon concentration, and sulfur S_t cause (net) damages $D_t(T_{1,t}, S_t, m_t)$ that we measure as a fraction of output

$$D_t(T_{1,t}, S_t, m_t) = 1 - \exp\left[-D_T(T_{1,t}) - D_G(S_t) - D_m(m_t) \right]. \tag{3}$$

We take the convex temperature-based damage function

$$D_T(T_{1,t}) = \xi_0 \exp\left(\xi_1 T_{1,t}\right) - \xi_0. \tag{4}$$

The damage parameter characterizes the percentage of global output lost at a 3°C temperature increase (the expected climate sensitivity).[1] The damages from the side effects of geoengineering are defined as

$$D_G(S_t) = d\, S_t, \tag{5}$$

making d the semi-elasticity of damages from stratospheric sulfur injections (the percentage loss of output resulting from an additional unit of sulfur injections). The parameter d includes operational costs. The net costs of an atmospheric carbon increase above preindustrial levels $(m_t - 1)$ are

$$D_m(m_t) = a\,(m_t - 1), \tag{6}$$

where a is the semi-elasticity of production with respect to changes in the carbon dioxide concentration. Costs include ocean-acidification and benefits include the fertilizer effect that increases plant production and crop yields. For our theoretic analysis we assume full depreciation of capital over the course of a decade, the model's time step, and the aggregate capital stock evolves as

$$K_{t+1} = Y_t \left[1 - D_t\left(T_{1,t}, S_t, m_t\right)\right] - C_t. \tag{7}$$

To account for the incomplete depreciation of capital over a decade, our quantifications make use of the ACE model's extended capital accumulation formula (Traeger 2021). A global social planner maximizes the infinite stream of consumption

$$\max_{C_t, E_t, S_t} \sum_{t=0}^{\infty} \beta^t \log(C_t) \tag{8}$$

[1]The climate sensitivity is the temperature response to a doubling of the preindustrial CO_2 concentration and we adobt the IPCC's (2021) current best guess in expectation. Temperature damages are convex and in technical terms ξ_0 characterizes the semi-elasticity of output to an exponential temperature increase above preindustrial levels, i.e., the percent of output lost in response of a unit increase of an exponential transformation of temperature. See Traeger (2021) for a detailed discussion of the functional form and calibrations to various estimates in the literature.

subject to equations (1)-(7), and some additional model details summarized in Appendix A. The parameter β denotes the utility discount factor.

2.2 Optimal policies in a deterministic world

This section provides a short overview of the main policy results of the global SolACE model from Meier and Traeger (2022). We use the deterministic outcome as a baseline and compare it to our results from the uncertainty analysis in the subsequent section. The optimal policy maximizes welfare with respect to the consumption rate, optimal labor distribution, capital distribution, fossil inputs, and sulfur deployment.

Sulfur deployment. The optimal level of sulfur deployment in the deterministic SolACE model is given by

$$S_t = \left(\frac{(1-n)\,\gamma\, f_3}{d + \gamma\, f_2} \right)^{\frac{1}{n}} m_t \tag{9}$$

with climate change impact $\gamma = \beta\, \xi_0\, \tilde{\sigma}$. Apart from the discount factor β, this climate impact is composed of the climate damage parameter ξ_0 (see equation 4) and a climate dynamics specifier $\tilde{\sigma}$. The climate dynamics specifier abbreviates a term reflecting the speed of the forcing response as well as ocean cooling. Its magnitude also depends on the discount factor, see equation (28) in Appendix A for its close-form solution.

The optimal level of sulfur deployment increases linearly in the atmospheric carbon concentration. The proportionality factor can be interpreted as the solar geoengineering propensity,

$$z^{det} \equiv \left(\frac{(1-n)\,\gamma\, f_3}{d + \gamma\, f_2} \right)^{\frac{1}{n}} \tag{10}$$

It includes the moderators and drivers of sulfur deployment. Sulfur deployment increases in the effectiveness of the cooling captured by f_3 and in the strength of the climate impact γ. Sulfur deployment falls in the geoengineering damages. The decrease of the cooling efficiency expressed by n has two counteracting impacts on optimal deployment. The term $1-n$ in the numerator reduces the deployment in response to the efficiency reduction, yet, the exponent increases with a cooling reduction, which can increase the propensity as long as it is sufficiently small.

Social Cost of Carbon. The SCC in money-measured consumption equivalents in the deterministic SolACE model is

$$SCC_t = \frac{Y_t^{net}}{M_{pre}} \left[\underbrace{a}_{\substack{\text{ocean} \\ \text{acid}}} + \underbrace{f_1 \gamma}_{\text{greenhouse}} \underbrace{- \left(\left(\frac{f_3}{z^n} - f_2 \right) \gamma - d \right) z^{det}}_{\text{geoengineering}} \right] \tilde{\phi}. \tag{11}$$

The solar geoengineering propensity z^{det} (see equation 10) reduces the SCC. And it does so more strongly, the higher the climate change impact $\gamma = \beta \, \xi_0 \, \tilde{\sigma}$ (which at the same time increases the base SCC proportional to f_1). The term $\tilde{\Phi}$ is a carbon cycle specific multiplier. It can be interpreted as a discounted sum over the decreasing fraction of a marginal ton of CO_2 emitted remaining in (or returning to) the atmosphere over the course of time, see Traeger (2021). The fraction $\frac{Y_t^{net}}{M_{pre}}$ sets the scale and units of the SCC. The square brackets characterize net damages and the term $\tilde{\phi}$ amplifies the SCC as a result of the long life-time of atmospheric CO_2 (carbon cycle). In the absence of geoengineering, most analytic integrated assessment models like ACE only contain a term corresponding to our $f_1\gamma$ reflecting the cost resulting from a temperature increase in the absence of climate engineering. Our additional term a represents the direct net damages from atmospheric CO_2 caused by ocean-acidification net of the land-based fertilization effect. The term in round brackets reduces the SCC as a result of solar geoengineering (the bracket is always positive). The inner bracket characterizes the net forcing reduction, a benefit, which is partially offset by solar geoengineering damages d. This reduction of the SCC increases concavely in the solar geoengineering propensity z^{det} (it shows up as well in the denominator because of decreasing efficiency).[2]

3 Geoengineering under Persistent Uncertainty

This section introduces long-term persistent uncertainty into the SolACE model. After introducing the policy maker's objective function (Bellman equation), we introduce uncertainty governing (i) damages from solar geoengineering, (ii) the forcing efficiency of sulfur, and (ii) climate change uncertainty. In this section's setting, the policy maker is aware of the stochastic nature of long-term damages and radiative forcing, but the nature of the setting limits his or her structural learning so that uncertainty remains persistent. We analyze optimal sulfur deployment and the SCC under such persistent long-term uncertainty.

[2]For a more detailed discussion see Meier and Traeger (2022) and Traeger (2021).

3.1 Objective

The policy maker optimizes the welfare of a representative agent. The policy variables are the consumption rate x_t, the optimal labor distribution $\boldsymbol{N}_t$, the normalized capital distribution $\boldsymbol{\mathcal{K}}_t$, the fossil inputs $\boldsymbol{E}_t$, and the sulfur deployment S_t which will be the object of our main focus. We consider a risk aversion optimization over an infinite time horizon. The representative households has log-utlity from consumption $u(C_t) = \log C_t$, which governs her (or the social planner's) elasticity of intertemporal substitution (EIS). Whereas an EIS of unity might be defensible for intertemporal substitution,[3] it is far too high to capture risk aversion. Thus, we disentangle risk aversion from the EIS and calibrate it to the asset pricing literature following Traeger (2018). The approach results in the Bellman equation

$$V_t(\cdot) \quad = \quad \max_{x_t, \boldsymbol{N}_t, \boldsymbol{\mathcal{K}}_t, \boldsymbol{E}_t, S_t} \log\big(C_t(x_t, \boldsymbol{N}_t, \boldsymbol{\mathcal{K}}_t, \boldsymbol{E}_t, S_t)\big) \; + \; \frac{\beta}{\alpha} \log\Big(\mathbb{E}_t \exp[\alpha\, V_{t+1}(\cdot)]\Big). \quad (12)$$

The parameter β captures utility discounting and α captures intrinsic risk loving. As such, α will generally be negative. The limit of $\alpha = 0$ corresponds to the standard Bellman equation where risk aversion is simply the inverse of the EIS (so unity). Setting $\alpha = -1$ corresponds to a disentangled Arrow-Pratt coefficient of *relative* risk aversion of approximately 8 and will be our base value Traeger (2018). The reader might recognize the expectation $\mathbb{E}_t \exp[\alpha V(\cdot)]$, with α negative, as constant (absolute) risk aversion aggregation. Here, it is applied to uncertainty over future uncertainty welfare as measured by the value function and, thus, measure risk aversion with respect to welfare gains and losses.[4] In the context of Epstein-Zin preference, α measures the difference between a decision maker's Arrow-Pratt risk aversion to uncertainty and her mere desire to smooth consumption over time. See (intrinsic risk aversion). See Traeger (2019) for a detailed and axiomatic discussion of intrinsic aversion to risk, which is identified in the data by a large literature on asset pricing and long-run risk.

Equation (12) suppresses the state variables that form the arguments of the value function and whose evolution depends on the control variables: consumption rate x_t, labor distribution over sectors $\boldsymbol{N}_t$ (a vector), capital distribution over sectors $\boldsymbol{\mathcal{K}}_t$ (a vector), and

[3] The standard macroeconomic literature suggests a lower elasticity of intertemporal substitution, yet the asset pricing and macro finance literature suggests a higher elasticity disentangling the EIS from risk aversion as well do here.

[4] The term $\frac{1}{\alpha}\log$ converts the expectation back into utility values where the α cancels for deterministic contributions. We emphasize that, despite the look of it, the exponential aggregator arises in the limit of taking the EIS to unity under log-utility in the more general Epstein and Zin (1991) setting.

primary energy inputs $\boldsymbol{E}_t$ (a vector containing both fossil and renewable energy), and the sulfur deployment S_t.

3.2 Damage uncertainty

The potential damages from sulfur-based geoengineering include changes in the precipitation patterns, a reduction in the upper ozone layer, acid precipitation and sulfur deposition (Crutzen 2006, Heckendorn et al. 2009, Keith and MacMartin 2015). Quantifying the adverse consequences of sulfur-based geoengineering are difficult given the lack of comparable experiments apart from a few volcanic explosions. Some authors, for example Moreno-Cruz and Keith (2013), therefore analyze optimal policy as a function of the damage parameter. Others make explicit assumptions, acknowledging a limited or hardly existing empirical basis. Table 1 shows several of those estimates and their translation into the damage parameter d, specifying the fraction of global output lost per TgS. Assessments of operational costs to deploy the sulfur particles are both smaller and more reliable than damage estimates.

Table 1: Damage uncertainty (Meier and Traeger 2022)

Authors	**Assumption**	d (per TgS)
Emmerling and Tavoni (2018b)	Consumption loss of 3% compensating each 3.5W/m^2 of forcing	0.1%
Goes et al. (2011a)	GDP loss between 0 and 5% per forcing equivalent to a doubling CO_2 forcing	0-0.17%
Heutel et al. (2018)	GDP loss of 3% for resetting forcing to the preindustrial level	0.21%

We incorporate the uncertainty of damages from solar geoengineering by adjusting the damage equation (5) as follows

$$D(S_t) = dS_t + \pi_t^d \tag{13}$$

where the parameter d continues to characterize the present best guess for geoengineering damages and the first term mirrors the deterministic model. The stochastic process π_t^d is itself a function of sulfur deployment and follows the equation

$$\pi_{t+1}^d = \epsilon_t^d \sqrt{S_t} + \Gamma^d \pi_t^d. \tag{14}$$

In every period $\epsilon_t^d \sim \mathcal{N}(0, \sigma_d^2)$ is a normally distributed mean-zero shock. The first term in equation (14) generates damage uncertainty whose variance increases linearly in sulfur

use (the square of $\sqrt{S_t}$). The second term in equation (14) makes damage uncertainty a persistent process. Realizations of current shocks correlate highly with future shocks as they most importantly represent learning about true damages apart from some stochastic fluctuations. High damage persistence is captured by a relatively large autoregressive coefficient Γ^d. The resulting one-step-ahead mean and variance of damags in equation (13) are

$$\mathbb{E}\, D(S_{t+1}) = \underbrace{dS_{t+1}}_{\textit{initially expected damage}} + \underbrace{\Gamma^d \Pi_t^d}_{\textit{shock persistence}} \quad \text{and} \quad \mathbb{V}\text{ar}\, D(S_{t+1}) = \underbrace{\sigma_d^2\, S_t}_{\textit{shock volatility}} \quad .$$

The structure of the stochastic process is common to model stock market risk and, in particular, long-run risk in asset pricing Bansal et al. (2014). Observing the current realization, the decision maker also updates his or her expectations over next period's damages as a result of the autoregressive shock-persistence. In that sense, the decision maker learns also in this setting of persistent uncertainty. However, the process is stationary and the uncertainty never fully resolves.

3.3 Uncertainty about cooling efficiency

The uncertainty governing the forcing efficiency is high and the instantaneous radiative forcing effect of sulfur injections varies strongly across different climate models (Niemeier and Timmreck 2015, Niemeier and Schmidt 2017, Kleinschmitt et al. 2018, Lawrence et al. 2018). In the real world, we experience major decreases around 1°C in global average surface temperature in response to some major vulcanic erruptions, such as mount Pinatobu in Indonesia in 1991 . The cooling potential does not only depend on the injection rate but also on the location of the injections. If sulfur particles are injected in the tropics, they spreads effectively towards the poles (Lawrence et al. 2018). As a consequence, it is impossible to do regional climate management using stratospheric geoengineering without spillovers to the other regions. Recent studies suggest that it might be possible to optimize the geographic distribution of the cooling by varying the altitude, latitude and season of injections (Visioni et al. 2019, Dai et al. 2018, Jones et al. 2018, MacMartin et al. 2017, Kravitz et al. 2017). The literature also proposed alternative aerosols like alumina and diamond particles (Weisenstein et al. 2015, Dykema et al. 2016), calcite or limestone (Keith et al. 2016). Given the lack of a natural experiment with such aerosols, our knowledge about the resulting forcing effect is even more limited.

We incorporate the uncertainty governing the cooling efficiency of stratospheric sulfur

by adjusting the deterministic radiative forcing equation (2) as follows

$$F_t(m_t, S_t) = \frac{\eta}{\log(2)} \log\left(f_0 + f_1\, m_t + \left(f_2 - f_3\left(\frac{m_t}{S_t}\right)^n\right) S_t + \pi_t^{fl} + \pi_t^{fn}\right), \tag{15}$$

where we introduced the stochastic process π_t^{fl} following

$$\pi_{t+1}^{fl} = \epsilon_t^{fl}\sqrt{S_t} + \Gamma^{fl}\,\pi_t^{fl} \quad \text{with} \quad \mathbb{E}_t\,\pi_{t+1}^{fl} = \Gamma^{fl}\,\pi_t^{fl} \quad \text{and} \quad \mathbb{V}\text{ar}_t\,\pi_{t+1}^{fl} = \sigma_f^2 S_t. \tag{16}$$

Once again, a mean-zero iid shock $\epsilon_t^{fl} \sim \mathcal{N}(0,\, \sigma_f^2)$ governs the first term and implies a variance that scales linearly in sulfur deployment. The second term makes the uncertainty persistent with the autoregressive coefficient Γ^{fl}.

The stochastic process in equation (16) scales the uncertainty linearly with sulfur deployment. As we explain in section 2.1 and see in equation (16) the main part of the actual cooling is a non-linear contribution that increases non-linearly with sulfur deployment as well as the prevailing CO_2[5] Therefore, we also introduce uncertainty that scales nonlinearly in these contributions following a second autoregressive stochastic process

$$\pi_{t+1}^{fn} = \epsilon_t^{fn}\sqrt{\left(\frac{m_t}{S_t}\right)^n S_t} + \Gamma^{fn}\,\pi_t^{fn} \quad \text{with} \quad \mathbb{E}_t\,\pi_{t+1}^{fn} = \Gamma^{fn}\,\pi_t^{fn} \quad \text{and} \quad \mathbb{V}\text{ar}_t\,\pi_{t+1}^{fn} = \sigma_f^2 m_t^n S_t^{1-n}. \tag{17}$$

whose shock variance scales with m_t^n and S_t^{1-n}, similar to that of the main deterministic forcing contribution. As with damage uncertainty, the decision maker can expect to learn from current shocks about the future, but uncertainty persists and never fully resolves.

3.4 Climate change uncertainty

Finally, we introduce uncertainty governing climate change itself. We include uncertainty about the temperature response to atmospheric CO_2 concentrations because these uncertainties could potentially make solar geoengineering more worthwhile. For the base uncertainty governing climate change we rely directly on Traeger (2018). He models the uncertain temperature response to atmospheric CO_2 using a shifted autoregressive gamma process z_t and we adopt process and calibration from the paper. We summarize details of this model in Appendix C, which also states mean and variance of the process z_t. In

[5]We remind the reader that the non-linear CO_2 interaction results from expressing sulfurs cooling effect in terms of CO_2 equivalent forcing, see Meier and Traeger (2022) for an extended discussion and transformation into generic forcing units.

addition to the process characterizing basic climate change uncertainty, we have to once again consider the interaction between CO_2's climate forcing and sulfur's cooling in the radiative forcing equation, which we further extend to the form

$$F_t(m_t, S_t) = \frac{\eta}{\log(2)} \log\left(f_0 + f_1\, m_t + \left(f_2 - f_3\left(\frac{m_t}{S_t}\right)^n\right) S_t + \pi_t^{fl} + \pi_t^{fn} + z_{t+1} + \pi_t^{cn}\right). \quad (18)$$

The process π_t^{cn} is the exact analogue of equation (17) again modeling uncertainty in the nonlinear forcing term that captures the interaction between sulfur and CO_2 in their temperature impact

$$\pi_{t+1}^{cn} = \epsilon_t^{cn}\sqrt{\left(\frac{m_t}{S_t}\right)^n S_t} + \Gamma^{cn}\,\pi_t^{cn} \quad \text{with} \quad \mathbb{E}_t\,\pi_{t+1}^{cn} = \Gamma^{cn}\,\pi_t^{cn} \quad \text{and} \quad \mathbb{V}\text{ar}_t\,\pi_{t+1}^{cn} = \sigma_f^2 m_t^n S_t^{1-n}. \quad (19)$$

Importantly, the forcing impact of this new nonlinear interaction term π_t^{cn} and that of the earlier stochastic process π_t^{fn} characterized in equation (17) are unlikely to be independent. Thus far, we have silently assumed that all one-step-ahead shock increments $\epsilon_t^d, \epsilon_t^{fl}, \epsilon_t^{fn}$, and z_t are independent. When it comes to ϵ_t^{cn}, we assume that the shock is generally correlated with the increment ϵ_t^{fn} as both together characterize the uncertainty governing the interaction between sulfur's cooling and CO_2's warming. We denote the correlation coefficient between the two by ρ. Both within a given model and across different models there can be uncertain physical processes or model differences that would offset each others stochastic shocks to the interaction term or that reinforce the uncertainty.

3.5 Optimal sulfur deployment

Appendix B solves the intertemporal optimization problem of optimal sulfur deployment. The optimal deployment strategy foresees future shock distributions and the persistence of shocks and our approach solves the infinite horizon stochastic fix point problem. As in the deterministic setting, we find that optimal slfur deployment increases linearly in the atmospheric carbon concentration. The crucial response to uncertainty lies in the

geoengineering propensity z^{unc}, i.e., the deployment per unit of atmospheric CO_2

$$S_t^{unc} = m_t \times \underbrace{\left(\frac{(1-n)\gamma f_3 - \frac{-\alpha\beta(1-n)}{(1-\beta\kappa)}\frac{\gamma^2}{2}\left[\overbrace{\frac{(\sigma^{fn})^2}{(1-\beta\Gamma^{fn})^2}}^{\text{geo nonlinear}} + \overbrace{\frac{2\rho\sigma^{fn}\sigma^{cn}}{(1-\beta\Gamma^{fn})(1-\beta\Gamma^{cn})}}^{\text{correlation geo and clim}} + \overbrace{\frac{(\sigma^{cn})^2}{(1-\beta\Gamma^{cn})^2}}^{\text{clim interaction}} \right]}{d + \gamma f_2 + \frac{-\alpha\beta}{2(1-\beta\kappa)}\left[\underbrace{\frac{(\sigma^d)^2}{(1-\beta\Gamma^d)^2}}_{\text{damage uncertainty}} + \underbrace{\frac{\gamma^2(\sigma^{fl})^2}{(1-\beta\Gamma^{fl})^2}}_{\text{geo linear}} \right]} \right)^{\frac{1}{n}}}_{\equiv z^{unc}}$$

The initial terms in the numerator and denominator of the geoengineering propensity z^{unc} remain the same as in the deterministic setting, see equation (11). Uncertainty introduces the terms proportional to risk aversion $-\alpha > 0$. These terms reduce the numerator and increase the denominator. Thus, all uncertainty contributions suppress sulfur deployment. We start by interpreting the contribution characterizing damage uncertainty. Similarly to the best guess damage parameter d, it increases the denominator. The uncertainty effect is proportional to the risk aversion weighted variance $-\alpha(\sigma^d)^2$, and it grows with the patience weighted persistence of the shocks (autocorrelation) $(1-\beta\Gamma^{fl})^2$. If the policy maker is patient and the uncertainty is persistent, then this factor substantially amplifies the policy maker's concern for uncertainty trigger by risk aversion and thos variance. We note that the persistence Γ^d 'physically' increases the long-run risk as the iid shocks to mean damages accumulate and build up long-term uncertainty. In contrast, the parameter β is the preference contribution and represents that the long-term buildup of uncertainty matters more for patient policy makers. The term $1 - \beta\kappa$ reflects the intertemporal investment multiplier resulting from the intertemporal spill-over of the shocks through the economic production and investment process.

The cooling uncertainty scaling linearly in sulfur deployment delivers a structurally almost identical contribution with the same dependencies and amplifiers. The only difference is that the climate impact parameter γ translates the forcing uncertainty σ^{fl} into the "climate damage relief" before it is weighted by the decision maker's risk aversion. The same is true for the nonlinear forcing uncertainty that reduces the numerator. Here, the middle term picks up the correlation. Together, the three contributions always reduce optimal sulfur deployment. If the shocks are perfectly negatively correlated, then the contribution is smallest (potentially zero if both shocks have the same magnitude). The contribution is strongest for perfectly positively correlated shocks.

3.6 The impact on optimal mitigation: the Social Cost of Carbon

The uncertainties affect not only the optimal sulfur deployment, but also the incentives to reduce CO_2 emissions. The SCC reflects the long-term damage from releasing a marginal ton of CO_2 into the atmosphere. The SCC along the optimal trajectory coincides with the Pigovian tax on CO_2 emissions. The optimal carbon tax is directly affected by the uncertainty and indirectly affected by the reduction of the geoengineering propensity discussed above. The SCC in money-measured consumption equivalents under long-term uncertainty is

$$SCC^{unc} = \frac{Y_t^{net}}{M_{pre}} \Bigg(\gamma \left(f_1 + f_2\, z^{unc} - f_3 \left(z^{unc} \right)^{1-n} \right) + a + d\, z^{unc} \tag{20}$$

$$+ \frac{-\alpha\, \beta}{2} \Bigg[\underbrace{\frac{(\sigma^d)^2}{(1-\beta\ \Gamma^d)^2}}_{\text{damage uncertainty}} + \underbrace{\frac{\gamma^2\, (\sigma^{fl})^2}{(1-\beta\ \Gamma^{fl})^2}}_{\text{forcing uncertainty } fl} \Bigg] z^{unc} + \underbrace{\frac{\gamma}{\beta} \frac{1}{1-\beta\gamma^z} \Big(\epsilon(c) + \theta(c) \Big)}_{\text{climate change uncertainty } cn}$$

$$+ \frac{-\alpha\beta\gamma^2}{2} \Bigg[\underbrace{\frac{(\sigma^{fn})^2}{(1-\beta\ \Gamma^{fn})^2}}_{\text{geo nonlinear}} + \underbrace{\frac{2\rho\sigma^{fn}\sigma^{cn}}{(1-\beta\ \Gamma^{fn})(1-\beta\ \Gamma^{cn})}}_{\text{correlation geo and clim}} + \underbrace{\frac{(\sigma^{cn})^2}{(1-\beta\ \Gamma^{cn})^2}}_{\text{clim interaction}} \Bigg] \left(z^{unc} \right)^{1-n} \Bigg) \tilde{\phi}$$

Uncertainty increases the SCC in two different ways. First, the first line of the SCC resembles that of the deterministic model, see equation (11), but with the geoengineering propensity z^{unc} instead of z^{det}. As we discussed above, uncertainty reduces the geoengineering propensity. As a result, each unit of emitted CO_2 will be (partially) offset to a lesser degree and the first line of the SCC falls in all the contributions discussed in Section 3.5 though the decline in z^{unc}.

Second, uncertainty directly and additionally lowers the SCC as we see in the second and third line. These direct impacts are of the same form as those that we discussed in the context of sulfur deployment. They are proportional to the risk-aversion weighted variance $-\alpha\sigma^2 > 0$. Patience-weighted persistence amplifies these contributions. The uncertainties affecting radiative forcing is moreover translated into the relief of climate damages using the climate impact parameter γ. The nonlinear interaction uncertainty increases with the correlation of the uncertainty between the climate change and the cooling uncertainty or climate model misspecification.

4 Quickly Resolving Short-Term Uncertainty

The previous section focuses on slow moving long-term uncertainty. These small but highly persistent shocks reflect slow learning over a long-run future. The present section studies the case where uncertainty resolves quickly over the course of a decade, our model's time step. Such a quick resolution of uncertainty is particularly likely for the cooling effectiveness of solar geoengineering (its radiative forcing contribution). Our first section discusses the case of a normally distributed forcing parameter whose true value will resolve over the course of the current period. For this normal case, we can provide an insightful analytic formula. The subsequent section discusses the case of Gamma distributed forcing uncertainty and adds quickly resolving uncertainty of geoengineering damages. Both sections connect the quickly resolving short-term uncertainty with the persistent long-term uncertainty modeled in Section 3.

4.1 Cooling uncertainty (normally distributed)

The crucial forcing parameter in our model that hopefully resolves substantially over a decade of geoengineering is the forcing effectiveness parameter f_3 in equation (2). We assume $f_3 \sim \mathcal{N}(\mu, \sigma^2)$. In general, we cannot find fully analytic solutions for the optimal sulfur deployment or the optimal carbon tax. Appendix D derives the implicit equation determining optimal forcing levels. We derive an explicit analytic solution approximating sulfur's forcing non-linearity parameter by $n = \frac{2}{3}$ as compared to our estimated value of $n = 0.69$. Then we can explicitly spell out the dependence of optimal sulfur deployment on all other model parameters. The resulting optimal sulfur deployment rate in the presence of quickly resolving cooling uncertainty is

$$S_0 = z^{unc} \left(\sqrt{1+Q^2} - Q \right)^3 m_0 \qquad \text{with} \qquad Q = \frac{-\alpha\gamma}{\beta(1-\beta\,\kappa)} \, \frac{\sigma^2}{2\mu} \left(\frac{(z^{lin})^2}{z^{joint}} \right)^{\frac{1}{3}} m_0, \quad (21)$$

where we assume $\mu = f_3$ and z^{lin} is the geoengineering propensity in the absence of the non-linear forcing and climate uncertainty where only the stochastic processes π_t^d and π_t^{fl} defined in equations (14) and (16) contribute persistent long-run uncertainty. The novel term Q is proportional to the variance σ^2 characterizing short-term uncertainty. If the short-term uncertainty vanishes so does Q and equation (21) returns the original sulfur control rule $S_0 = z^{unc}\, m_0$. As we increase the uncertainty, the term Q reduces optimal

sulfur deployment.[6] Apart from the short-term forcing uncertainty, the term Q also increases proportional to the prevailing CO_2 level. Thus, the uncertainty turns the linear relation between atmospheric CO_2 and optimal sulfur deployment concave. By limiting the linear increase of sulfur deployment with the atmospheric carbon concentration short-term uncertainty reduces the deployment sensitivity historic emissions.

In addition, the deployment falls in risk aversion $-\alpha > 0$ and the climate impact γ that translates forcing uncertainty into economic damages. The multiplier $1 - \beta\kappa$ in Q's denominator reflects again the intertemporal investment multiplier resulting from the intertemporal spill-over of the shocks through the economic production and investment. Finally, the damping is larger if more of the geoengineering propensity is driven by the uncertainty processes π_t^d and π_t^{fl} whose variance scales linearly in deployment as compared to nonlinearly processes π_t^{fn} and π_t^{fn}.

4.2 Gamma distributed Cooling & damage uncertainty

It is less obvious whether the uncertainty governing climate damages resolves as quickly as the uncertainty governing the sulfur-based cooling. That said, it is reasonable to assume that the first decade of geoengineering will substantially reduce some of the damage uncertainties, while other uncertainties governing long-term and cumulative impacts will persist. The present setting also splits the uncertainty over damages from geoengineering into quickly resolving short-term versus persistent long-term uncertainty.

So far, we have assumed that all random variables are normally distributed. Absent better knowledge, a normal distribution stands to reason. However, a left-bounded distribution might be similarly reasonable if we are confident that damages are non-negative and that sulfur-based geoengineering cannot lead to an increase in radiative forcing (warm the planet). In addition, the normal distribution neither exhibits skew nor kurtosis. In order to test the implications of the normal distribution's symmetry assumption as well as the absence of kurtosis (or 'fatness') we analyze the policy impact of gamma distributed forcing and damage uncertainty. We assume that sulfur's forcing uncertainty is governed by $f_3 \sim \Gamma(\bar{k}^{fl}, \theta^{fl})$ with shape parameter $\bar{k}^{fl}$ and a scale parameter θ^{fl}. We assume that geoengineering damages are distributed $d \sim \Gamma(\bar{k}^d, \theta^d)$ with shape parameter $\bar{k}^d$ and scale parameter θ^d. We assume that both random variables are independently distributed and resolve during the first period. The shape and the scale parameters are functions of the expected values μ_i (the deterministic model's best guesses) and the corresponding

[6] It is easy to see that the term $(\sqrt{1+Q^2}-Q)^3$ converges monotonically to zero as $Q \to \infty$. However, such high Q values lie far outside of our calibration.

uncertainties as characterized by the variances σ_i^2

$$\theta^i = \frac{\sigma_i^2}{\mu_i} \quad \text{and} \quad k^i = \frac{\mu_i}{\theta^i} \quad \text{for } i \in \{f, d\} \tag{22}$$

Introducing damage uncertainty implies that the uncertainty already has a direct impact on current period consumption and utility. The standard timing of the Bellman equation would not permit such uncertainty as current controls are optimized under uncertainty only over next period states but not uncertainty governing current period consumption. With a decadal time step, and given our present ignorance about geoengineering damages, we want to analyze the case where decisions about the first implementation of large scale geoengineering are made under immediate uncertainty about geoengineering damages. As a result, we have to introduce uncertainty governing already the upcoming period and modify the Bellman equation to

$$V_t(\cdot) = \max_{x_t, \boldsymbol{N}_t, \boldsymbol{\mathcal{K}}_t, \boldsymbol{E}_t, S_t} \mathbb{E}_0 \exp\left[\alpha \left(\log\left(C_t(x_t, \boldsymbol{N}_t, \boldsymbol{\mathcal{K}}_t, \boldsymbol{E}_t, S_t)\right) + \frac{\beta}{\alpha} \log\Big(\mathbb{E}_t \exp[\alpha\, V_{t+1}(\cdot)]\Big)\right)\right].$$

In evaluating equation (71), we assume that the first instance of long-term uncertainty resolves in period 1 and, thus, is governed by the expected value operator $\mathbb{E}_1$ at the end of period 1 (or the beginning of period 2). The short-term uncertainty, i.e., our gamma distributed parameters d and f_3, are governed by the immediate uncertainty evaluated by $\mathbb{E}_0$.

There is no general analytic solution for the optimal sulfur level. Analyzing only one of the two uncertainties at a time, we can obtain analytic solutions under the assumption that $n = \frac{2}{3}$ (as compared to our estimated $n = 0.69$). However, these solutions are the roots of a cubic and quartic functions and are no longer very insightful. Appendix D.1 derives the implicit equation defining optimal sulfur deployment

5 Quantification and Discussion of Anticipated Learning

This section quantifies the effects of persistent long-run and quickly resolving short-term uncertainty on optimal sulfur deployment and the incentive to mitigate. After summarizing our calibration, we show and compare the impact of the various uncertainties on optimal sulfur deployment. Subsequently, we discuss the effects of learning and optimal deployment after the short-term uncertainty has resolved. Finally, we present the impact of solar geoengineering on the SCC, i.e., the incentive to mitigate.

5.1 Calibration

The deterministic model components and our expected parameter values rely on the calibration in Meier and Traeger (2022). Table 2 summarizes the main SolACE parameters. As for the regions in the cited SolACE model, we have scaled up global warming damages

Table 2: Parameter values from deterministic SolACE model.

β	ξ_0	ξ_0^{higher}	$\tilde{\sigma}$	n	f_3	d
0.986^{10}	3.2%	6.3%	0.63	0.69	0.46	0.1%

by 50% as compared to the DICE model. We refer to Traeger (2021) for a detailed discussion of our climate damage function's relation to the various versions of Nordhaus's (2019) DICE model. Our 50% increase is based on increasing evidence that that DICE damages have been calibrated too low, as well as the paying more emphasis on matching the initial damage convexity of DICE's quadratic damage function rather than merely levels, which increases ξ_0. The parameter ξ_0 characterizes the damages in percent of world output at a 3°C temperature increase over preindustrial levels (expected climate sensitivity). When matching levels, the damage function is initially less convex than the common quadratic form and eventually more convex. The value is still very low as compared to some recent estimates Burke et al. (2015), Howard and Sterner (2017), Newell et al. (2021) and our choice purposefully stacks the cards against geoengineering. In addition to our base choice, we will assess geoengineering for climate change induced damages of $\xi = 6.3\%$ of world output at a 3°C warming, the expected damages of Traeger (2018), still a conservative but maybe more reasonable value in view of the recent literature.

Much of our analysis evaluates the option to deploy sulfur in 2050 in a scenario where atmospheric temperature has reached 1.8° above preindustrial and the atmospheric carbon concentrations are 1.8 times the preindustrial level. This scenario is based on Meier and Traeger's (2022) simulation where policy makers incorporate regional but not global climate damages. Having crossed the 1.5° target and approaching the 2° target seems a natural point to assess the option of geoengineering. To assess our sulfur deployment after uncertainty resolves, we have to model emissions jointly with sulfur deployemnt. For this purpose, we use the global version of the updated RICE model in Meier and Traeger (2022). Our choice of the production sectors merely impacts our CO_2 emissions. As a result, this choice has an almost negligible impact on the results we present. Our choices of the climate damage parameter result in the climate impact parameters $\gamma = \beta\,\xi_0\,\tilde{\sigma} = 1.7\%$ for the base case and $\gamma = 3.5\%$ for the scenario with higher climate damages. For an

overview of all economic and climate model parameters we refer to Meier and Traeger (2022). We take the calibration of risk aversion of $\alpha = -1$ and the calibration of long-run climate change (base) uncertainty from Traeger (2018). Given a decadal time step, we set the autoregressive uncertainty persistence parameter to $\Gamma^d = \Gamma^{fl} = \Gamma^{fn} = \Gamma^{cn} = 0.75$. The autoregressive parameter of the base climate uncertainty model is slightly higher with a decadal autoregression of $\Gamma = 0.8$ suggesting even more persistence in climate uncertainty. These choices are loosely based on comparisons to a slow Bayesian learning model discussed in Traeger (2018). We list our values for the new parameters governing uncertainty in Tables 3 (damage uncertainty) and 4 (forcing uncertainty).

Our best guess for geoengineering discussed in Section 3.2 is $d = 0.1\%$ of world output per TgS (million tons of annual sulfur deployment). We pick a standard deviation characterizing short-run damage uncertainty of $\sigma^{ds} = 0.05\%$. This choice is mostly inspired by (i) acknowledging that we know very little about the quantitative impact of the resulting damages and (ii) using the pdf depicted on the right of Figure 1 as a guide to judge the magnitude of uncertainty. The pdf still gives considerable mass to double the expected damages and has a fat tail. Our extreme damage scenario further increases the variance by doubling the standard deviation. The dash-dotted line in Figure 1 shows that such a further increase in uncertainty has a somewhat extreme impact on the shape of the Gamma distribution. In order to maintain the expected value, the resulting fat tails can only be compensated for by placing a lot of mass on vanishingly small damages. Our choices for the damage variance and expectation pin down the shape and scale parameters of the Gamma distribution by equation (22). In contrast to short-term uncertainty,

Table 3: Damage uncertainty parameters.

long-run			short-term		high
σ^d	Π_0^d	Γ^d	μ^d	σ^{ds}	σ^{ds}_{high}
0.01%	0	0.75	0.1%	0.05%	0.1%

persistent uncertainty builds up over time to a factor of $\frac{1}{1-\Gamma^d} = 4$ times the magnitude of each period's uncertainty σ^d. Thus, our choice of $\sigma^d = 0.01\%$ generates a distribution giving rise to generous long-run uncertainty over the unknown damages from geoengineering. Anticipating deployment levels in the magnitude of a few TgS, the long-run uncertainty will be larger than the short-run uncertainty. Overall, we think that our uncertainty choices stack the cards against geoengineering: we assume high uncertainty levels already individually for both short-run and long-run uncertainty, and these add up in characterizing today's uncertainty over the potential damages caused by geoengineering. Finally, we

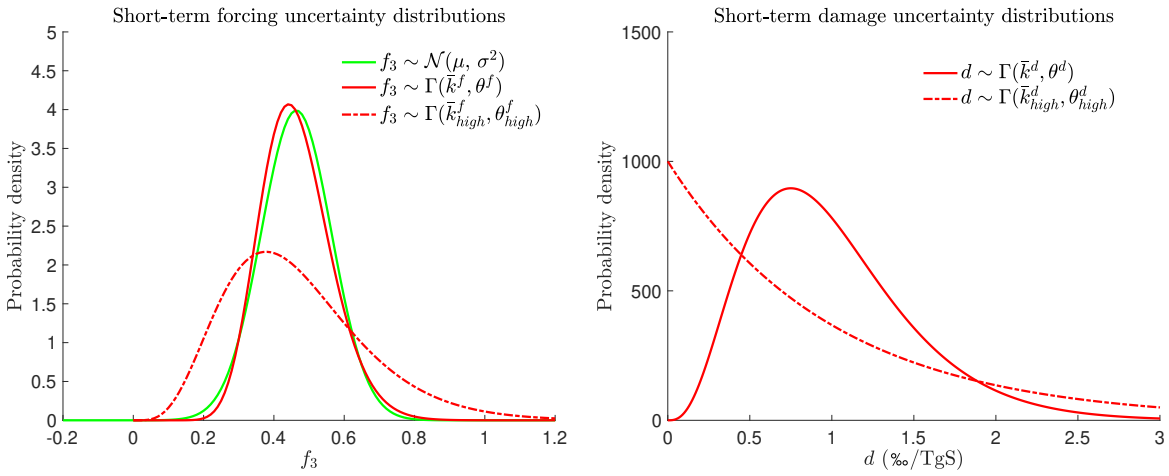

(a) Forcing uncertainty f_3 (b) Damage uncertainty d

Figure 1: Probability density functions for the different specifications of short-term uncertainty stated in Table 3 and 4. The damage coefficient is in per mille (so 10^{-3}) of global world output per TgS (one million tons of sulfur deployed annually).

set the initial deviation from today's expectation $\Pi_0^d = 0$, also aligning today's long-run expectations with our damage guesstimate of $d = 0.1\%$.

We have slightly more information to calibrate sulfur's forcing uncertainty as a result of the recent G6 Solar Geoengineering Model Intercomparison Project. Based on personal communications with one of the authors of Visioni et al. (2021), we found that the relative forcing deviation across models at a 5 TgS annual deployment was approximately $\pm 40\%$ of the average forcing effect.[7] Given that our epistemological uncertainty exceeds the model differences, we calibrate our uncertainty to about $\pm 50\%$ of the average cooling at a 5TgS deployment. For higher deployment levels our model's uncertainty exceeds the model variation more generously. This uncertainty calibration leads to $\sigma^{fs} = 0.1$. For our high uncertainty scenario, we again double the standard deviation of the base scenario resulting in $\sigma^{fs}_{high} = 0.2$. We set the long-run persistent uncertainty to $\sigma^{fl}\sigma^{fn} = \sigma^{cn} = 0.025$, which again builds up over time to a long-run uncertainty about four times as high. The expected value remains $\mu^{fs} = f_3^{det} = 0.46$ and initial deviation is $\Pi_0^d = 0$. We assume that the uncertainty between the nonlinear interaction terms stemming from climate uncertainty and cooling uncertainty are moderately positively correlated with $\rho = 0.5$. Figure 1a on the left depicts the implied probability density functions for our short-term forcing uncertainty parameter f_3. The difference between the normal and the gamma distribution

[7]We are extremely grateful to Daniele Visioni for his help and for sharing graphs from ongoing work based on the cited article's data that we used in our calibration.

Table 4: Forcing uncertainty parameters.

long-run							short-term		high
σ^{fl}	σ^{fn}	σ^{cn}	Π_0^d	Γ^{fl}	Γ^{fn}	Γ^{cn}	μ^{fs}	σ^{fs}	σ^{fs}_{high}
0.025	0.025	0.025	0	0.75	0.75	0.75	0.46	0.1	0.2

in the base calibration is quite small. The asymmetry of the Gamma distribution becomes more pronounced in the high uncertainty scenario.

5.2 Optimal Sulfur Deployment, Learning, and SCC

Figure 2 shows the optimal sulfur deployment as a function of the global atmospheric carbon concentration relative to preindustiral levels. If climate damages are judged moderate, optimal deployment levels are in the order of 5TgS or 5 million tons sulfur per year. This deployment level corresponds to approximately 125 Boeing 747 flights deploying the sulfur every day. [8] These stratospheric sulfur injections are small compared to the approximately 136 TgS/yr of sulfur emitted into the air as a result of fossil fuel combustion and industrial processes (Kravitz et al. 2009). The optimal deployment doubles if we judge climate damages to be more severe. The impact of uncertainty on deployment is small. The impact of long-run persistent uncertainty is negligible. The impact of quickly resolving short-term uncertainty is more notable and splits almost evenly between damage and forcing uncertainty. Here, anticipated structural learning delivers an additional incentive to "wait and see". We note that our learning is conditional only on deployment, not on the level of deployment. This assumption further stacks the cards against high levels of sulfur deployment. Nevertheless, we see that uncertainty and learning have only a mild impact on deployment. The difference between normally distributed and gamma distributed forcing uncertainty is negligible. Only the high uncertainty scenario reduces deployment more seriously, but even the reduction in this extreme uncertainty scenario is small relative to overall deployment.

Figure 3 shows the optimal deployment after learning. The future realizations of damages and cooling efficiency are uncertain. Therefore, we present a pdf characterizing the probability of different sulfur deployment levels.[9] We note that different combinations

[8] The planes actually deploy the sulfur in terms of sulfur dioxide, which doubles the elementary mass. A Boeing can not reach high enough, but can fuel fighter jets to bring the sulfur to the relevant altitudes. More likely, dedicated airplanes will be designed for the task.

[9] Our pdf discards realizations that would target a temperature below the preindustrial level. While extreme realizations might makes such a scenario reasonable, we do not consider our model suitable to discuss such extreme realizations.

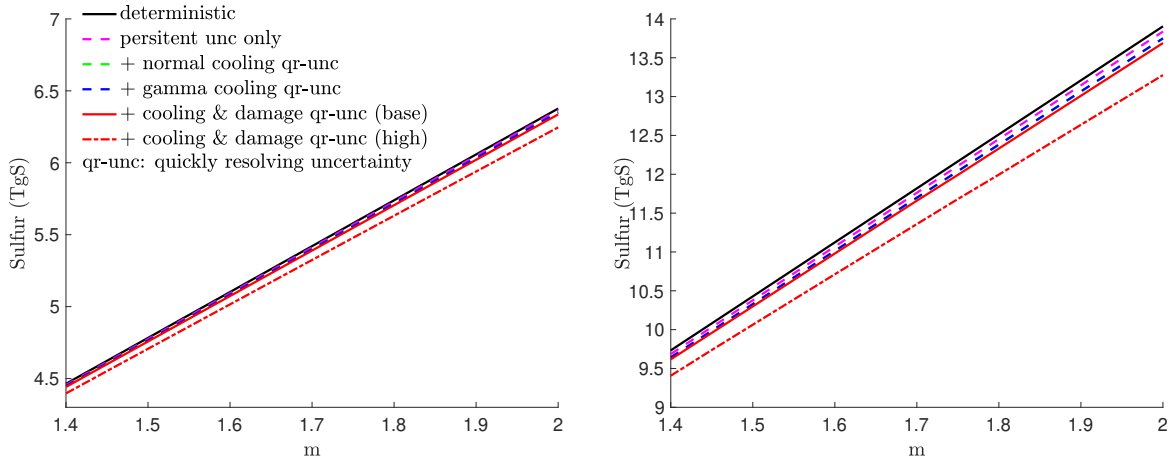

(a) Base case climate damages ($\xi_0 = 3.15\%$) (b) High climate damages ($\xi_0 = 6.3\%$)

Figure 2: Optimal sulfur deployment before the resolution of the quickly resolving short-term uncertainty (qr-unce) for two different climate damage specifications. All but the deterministic scenario contain persistent long-run uncertainty and the legend specifies the additional short-term 'qr'-uncertainty.

of geoengineering damages and cooling efficiency can lead to the same deployment levels. The lines characterize the density of the continuous distribution. The bars on the left represent the discrete probability of no sulfur deployment, which is 25% under the assumption of moderate climate damages and close to 10% in the case of higher climate damages. The range of deployment levels after uncertainty resolves (ex-post) covers a wide interval; both half and double the ex-ante deployment level still receive considerable weight. Our default simulation (blue line) requires that the net benefit of sulfur deployment has to exceed 0.1% of world output, otherwise geoengineering will not happen. Global geoengineering requires more than merely moving planes to the stratosphere. There are many stakeholders and different countries with strong views on the topic. Our threshold criterion captures that deployment will not happen unless the net benefit is large enough to make it worthwhile confronting some opposition. The dotted orange line represents ex-post deployment without such a political threshold criterion. We can see that the efficiency threshold shaves off some of the probability mass at relatively low deployment levels (turning them into no deployment).

In the scenario with moderate climate damages, the expected ex-ante net benefit of geoengineering is 0.19% of global world output. The expected ex-post net benefit is 0.28% of global output as a result of learning. We can show that the additional ex-post value derives from learning using the following experiment. We commit the policy maker's

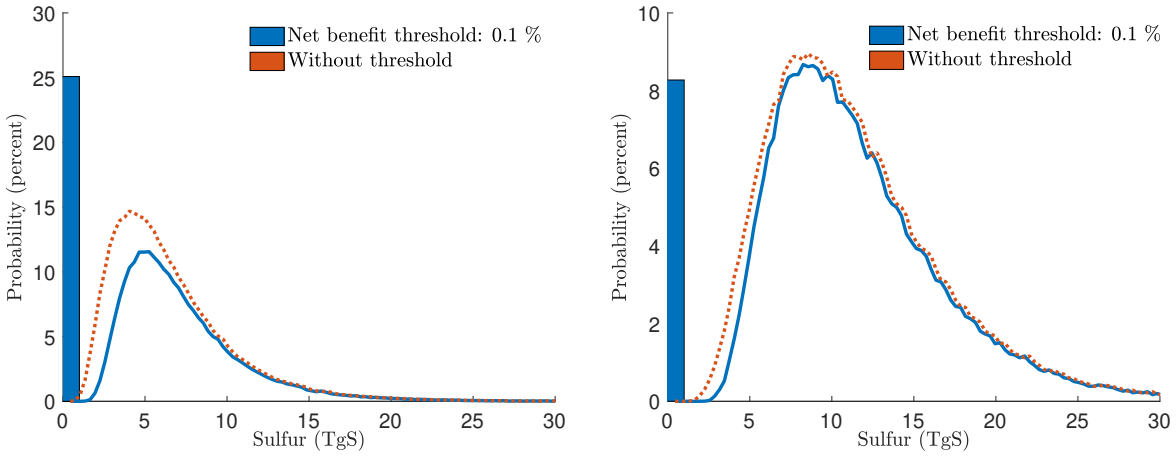

(a) Expost sulfur ($\xi_0 = 3.15\%$) (b) Expost sulfur ($\xi_0 = 6.3\%$)

Figure 3: Optimal sulfur deployment after the resolution of short-term uncertainty. The bar on the left has unit-width and depicts the discrete probability of foregoing geoengineering after the uncertainty resolved. The blue line assumes that geoengineering is only deployed if its net benefit exceeds 0.1% of world output, an assumption that chips away some of the probability mass for low sulfur deployment levels (orange-dotted line).

second period sulfur deployment to the sulfur level that would be optimal in the absence of learning, i.e., ex-ante optimal but in the second period when the actual realizations of short-term uncertainty already happened. Thus, we do not allow the policy maker to condition his or her deployment levels on the realizations. Then, ex-post net-benefits stay almost as low as in the ex-ante scenario. They are slightly higher because of a carbon stock and temperature increase from one period to the next (0.21%). We find that, under moderate climate damages, short-term uncertainty and, thus, realizations of damages generates a larger increase in ex-post value than the short-run uncertainty in cooling efficiency. This finding goes along with a higher variance of ex-post sulfur deployment under damage uncertainty (compared to cooling uncertainty). The decision maker gains more from conditioning optimal sulfur deployment on the realization of damages, and conditioning on realized damages makes a larger difference to optimal ex-post deployment.

The discussion above illustrates how the ability to learn gives a value to uncertainty. Ex-ante deployment under uncertainty is very similar to the deployment under certainty, where the deterministic model simply uses expected values for the different parameters and ignores the uncertainty. Yet, for geoengineering, we expect part of the uncertainty to resolve quickly. As a result, the decision maker can condition optimal deployment strategies on the learned information. Therefore, (quickly resolving) uncertainty can

increase the attractiveness of geoengineering if the decision maker is forward looking. Ex-ante and ex-post benefits increase to 0.48% and 0.62% of global world output when climate damages are judged more severe (or accounted for at a higher value). As the stakes increase, so does the net benefit of resolving uncertainty (the difference between the two values). Interestingly, under the higher climate damages, the ex-post increase of net benefits is as much driven by forcing uncertainty as it is driven by damage uncertainty (which dominates under lower climate damages). As global warming damages become more severe, cooling efficiency gains importance relative to geoengineering damages.

The SCC captures the incentive to mitigate greenhouse gases. Our base scenario with moderate climate damages has a present value SCC of 53$/tCO2 (USD per ton of carbon dioxide) in the absence of geoengineering. Introducing the option of sulfur-based geoengineering in a deterministic setting drops this value to 38$/tCO2, a substantial reduction in the incentive to mitigate. Our persistent long-run uncertainty increases the value to 40$/tCO2, again a rather minor impact of uncertainty in the 'ex-ante world', where we use equation (20) (which lacks the impact of quickly resolving uncertainty). The biggest SCC risk premium derives from our base climate uncertainty, a small part from forcing uncertainty, and damage uncertainty has close to no impact on the ex-ante SCC. For higher climate damages, the SCC without geoengineering is 100$/tCO2 and it falls to 58$/tCO2 with the option of geoengineering in a deterministic world. Persistent long-run uncertainty raises the SCC with geoengineering to 61$/tCO2 where once again the main contribution stems from climate change uncertainty. Overall, the reduction of the mitigation incentive triggered by the expected deployment of geoengineering is substantial and warrants the worries that solar geoengineering can interfere with mitigation. That said, also the reduced SCC under geoengineering is still far larger that actual carbon taxes or carbon prices in most of the world. Persistent long-run uncertainties slightly increase the SCC again, but only mildly so compared to the major drop triggered by the expected use of geoengineering.

Figure 4 depicts the optimal carbon tax and, thus, mitigation incentive after the short-term uncertainty has resolved. The discrete probability on the highest tax corresponds to the case of stopping geoengineering after the short-term uncertainty resolves. We see that this discrete probability relies on our assumption that policy makers only carry out geoengineering if its myopic net benefit exceeds a minimal threshold. This assumption shifts probability mass from the organge-dottet curve without such a threshold to the blue bar representing the optimal tax in the absence of geoengineering. Whereas the threshold requirement shaves Figure 3's sulfur deployment probability off smoothly, it cuts Figure

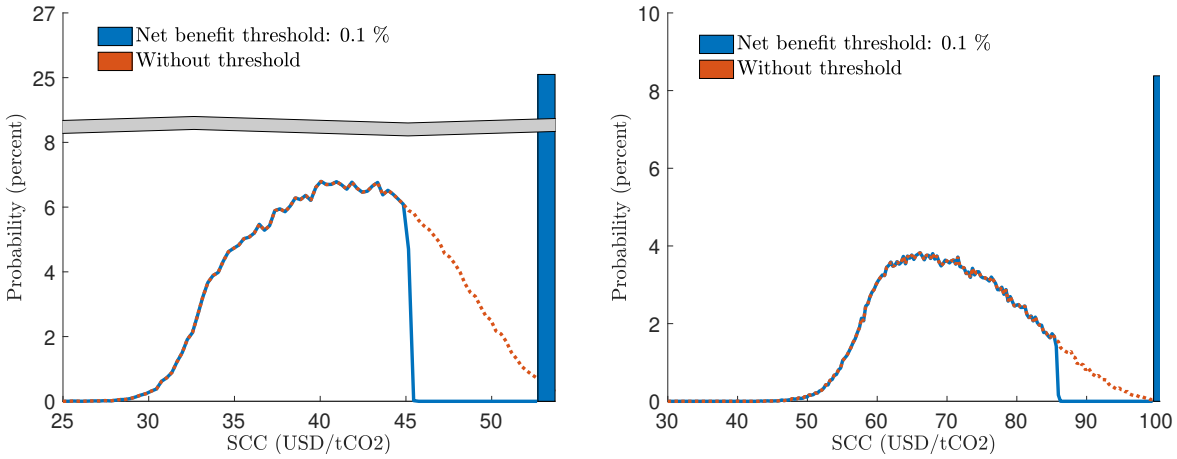

(a) Expost SCC ($\xi_0 = 3.15\%$) (b) Expost SCC ($\xi_0 = 6.3\%$)

Figure 4: Optimal carbon tax (SCC) after the resolution of short-term uncertainty. The bar on the right has unit-width and depicts the discrete probability of foregoing geoengineering, which triggers an SCC of 53$/tCO2 (left, moderate climate damages) and 100$/tCO2 (right, higher climate damgages). The blue line assumes that geoengineering is only deployed if its net benefit exceeds 0.1% of world output.

4's SCC distribution off sharply. The different combinations that just fail the myopic net benefit criterion also lead to the same SCC.

6 Conclusions

We examine the impacts of uncertainty on the deployment decision of solar geoengineering. We provide explicit rules for optimal deployment, analytic insights, and quantitative advice. Our findings support those of the deterministic literature. Geoengineering is a valuable measure to counteract global warming. It is hard to justify eliminating this option from our policy portfolio. Anticipating learning, uncertainty can even make sulfur deployment more attractive compared to deterministic models operating on best-guess assumptions.

We find that, despite major uncertainties, a large scale implementation of sulfur deployment is attractive, at least initially. Uncertainty slightly reduces the level of the initial deployment as compared to models that simply base the deployment decisions on best guess damages or cooling efficiency. This reduction increases in risk aversion, patience-weighted uncertainty persistence, and of course the level of uncertainty itself. It also increases slightly if the uncertainties governing sulfur-based cooling and climate change

warming are correlated. Finally, the uncertainty's impact on initial sulfur deployment is stronger if we can expect uncertainty to resolve quickly. Yet, in the end, the magnitude of this reduction is surprisingly small.

Our decision maker understands that he or she will learn from an initial large scale deployment. The decision maker's initial deployment strategy accounts for the value of learning. After the initial learning phase, we find a substantial likelihood that solar geoengineering will be discontinued. In our base scenario with rather moderate climate damages this probability is 25%. The probability falls to just under 10% in our scenario with higher climate damages. These values are based on an initial roll-out of solar geoengineering in 2050 under a 1.8°C warming. This scenario, simulated in a regionally strategic version of SolACE (Meier and Traeger 2022) is the type of scenario where geoengineering is discussed the most: we have already exceeded the 1.5°C scenario and are on the way to also exceed 2°C. Thus, while encouraging an initial trial of solar geoengineering, our model also warns against banking on solar geoengineering as a sole or reliable solution to the global warming problem.

Real-world policy makers often rely on – or are forced to adopt – cost-benefit criteria that are myopic instead of taking rational forward looking choices that incorporate a value of learning. We subject our deployment strategies to a one-period cost-benefit assessment rule that implements solar geoengineering only if the immediate climate change damage relief dominates the expected damages from geoengineering by a threshold of at least 0.1% of global output. Such a criterion does not prevent ex-ante deployment, but is partly responsible for discontinuing geoengineering after the learning phase. Ex-ante, sulfur-based solar geoengineering fails the myopic test if we double the threshold or evaluate deployment at today's warming level. By contrast, the expected post-learning (one-period) net-benefit clearly passes also more stringent threshold criteria. After the short-term uncertainty has resolved, the policy maker continues geoengineering only if it is worthwhile. Moreover, he or she will adjust the sulfur-deployment level to the observed realizations of expected damages and cooling efficiency, substantially raising expected ex-post net benefits over expected ex-ante net benefits.

We find that the incentive to mitigate greenhouse gas emissions falls substantially when we anticipate an initial deployment of solar geoengineering. The corresponding SCC falls by 25-40%, a drop that increases with the severity of climate damages. This reduction in the incentive to mitigate happens even if we anticipate that solar geoengineering might be a failure ex-post. The substantial probability that geoengineering will be discontinued after initial deployment adds an interesting twist to a wide-spread concern

in the scientific community. The concern is often connected to the metaphor of a slippery slope. We should not even research solar geoengineering because the mere research can discourage mitigation and put us under pressure to undertake geoengineering. Indeed, we find that ex-ante the expectations governing geoengineering substantially reduce the optimal mitigation effort, even for a perfectly rational and forward looking policy maker in an integrated assessment model with geoengineering and climate uncertainty. Yet, ex-post, there is a substantial likelihood that we end up in a world where we have reduced mitigation efforts ex-ante only to later revise the SCC back up realizing that solar geoengineering is not as beneficial as expected. If we are afraid of such a situation, it might not be smart to procrastinate on research or deployment. Before deployment and learning, expecting potential future benefits reduces mitigation incentives, not just for some myopic politician, but for a perfectly rational forward looking decision maker. Thus, it seems helpful not to procrastinate on research and testing bit to explore the options on the table and revise expectations.

Our calibration has stacked many cards against geoengineering. We assume rather moderate climate change damages and high levels of both long-run persistent and quickly resolving short-term uncertainty, governing the efficiency and damages of solar geoengineering. Moreover, our geoengineering damage uncertainty is fat-tailed. Yet, we find that a large scale deployment experiment of considerable duration is reasonable from the perspective of a rational forward looking decison maker as well as the perspective a myopic policy maker. Within our model, these findings are robust. We do not consider our model by itself a reasonable base to promote large scale experimentation. We can think of many more checks, including variations in functional forms and a more detailed analysis of optimal timing and magnitude of initial experiments. But we see our paper as an inspiration for more and result-open research on the economics of solar geoengineering – not despite but because of the uncertainties governing this important topic in a world that is not on a path to meet its climate targets.

References

Bahn, Olivier; Chesney, Marc; Gheyssens, Jonathan; Knutti, Reto, and Pana, Anca Claudia. Is there room for geoengineering in the optimal climate policy mix? Environmental Science & Policy, 48:67–76, 2015.

Bansal, Ravi; Kiku, Dana; Shaliastovich, Ivan, and Yaron, Amir. Volatility, the macroeconomy, and asset prices. The Journal of Finance, 69(6):2471–2511, 2014.

Biermann, Frank; Oomen, Jeroen; Gupta, Aarti; Ali, Saleem H; Conca, Ken; Hajer, Maarten A; Kashwan, Prakash; Kotzé, Louis J; Leach, Melissa; Messner, Dirk, et al. Solar geoengineering: The case for an international non-use agreement. Wiley Interdisciplinary Reviews: Climate Change, 13(3):e754, 2022.

Burke, Marshall; Hsiang, Solomon M, and Miguel, Edward. Global non-linear effect of temperature on economic production. Nature, 527(7577):235–239, 2015.

Crutzen, Paul J. Albedo enhancement by stratospheric sulfur injections: A contribution to resolve a policy dilemma? Climatic Change, 77(3-4):211–219, 2006.

Dai, Z.; Weisenstein, D. K., and Keith, D. W. Tailoring Meridional and Seasonal Radiative Forcing by Sulfate Aerosol Solar Geoengineering. Geophysical Research Letters, 45(2): 1030–1039, 2018.

Dykema, J. A.; Keith, D. W., and Keutsch, F. N. Improved aerosol radiative properties as a foundation for solar geoengineering risk assessment. Geophysical Research Letters, 43(14):7758–7766, 2016.

Emmerling, Johannes and Tavoni, Massimo. Climate Engineering and Abatement: A 'flat' Relationship Under Uncertainty. Environmental and Resource Economics, 69(2): 395–415, 2018a.

Emmerling, Johannes and Tavoni, Massimo. Exploration of the interactions between mitigation and solar radiation management in cooperative and non-cooperative international governance settings. Global Environmental Change, 53:244–251, 2018b.

Epstein, Larry G and Zin, Stanley E. Substitution, risk aversion, and the temporal behavior of consumption and asset returns: An empirical analysis. Journal of Political Economy, 99(2):263–86, April 1991.

Flegal, Jane A; Hubert, Anna-Maria; Morrow, David R, and Moreno-Cruz, Juan B. Solar geoengineering: Social science, legal, ethical, and economic frameworks. Annual Review of Environment and Resources, 44:399–423, 2019.

Gerlagh, Reyer and Liski, Matti. Carbon Prices for the Next Hundred Years. Economic Journal, 128(609):728–757, 2018.

Goes, Marlos; Tuana, Nancy, and Keller, Klaus. The economics (or lack thereof) of aerosol geoengineering. Climatic Change, 109(3-4):719–744, 2011a.

Goes, Marlos; Tuana, Nancy, and Keller, Klaus. The economics (or lack thereof) of aerosol geoengineering. Climatic change, 109(3):719–744, 2011b.

Golosov, Mikhail; Hassler, John; Krusell, Per, and Tsyvinski, Aleh. Optimal Taxes on Fossil Fuel in General Equilibrium. Econometrica, 82(1):41–88, 2014.

Gourieroux, Christian and Jasiak, Joann. Autoregressive gamma processes. Journal of Forecasting, 25:129–152, 2006.

Harding, Anthony and Moreno-Cruz, Juan B. Solar geoengineering economics: From incredible to inevitable and half-way back. Earth's Future, 4(12):569–577, 2016.

Heckendorn, P.; Weisenstein, D.; Fueglistaler, S.; Luo, B. P.; Rozanov, E.; Schraner, M.; Thomason, L. W., and Peter, T. The impact of geoengineering aerosols on stratospheric temperature and ozone. Environmental Research Letters, 4(4), 2009.

Helwegen, Koen G; Wieners, Claudia E; Frank, Jason E, and Dijkstra, Henk A. Complementing co 2 emission reduction by solar radiation management might strongly enhance future welfare. Earth System Dynamics, 10(3):453–472, 2019.

Heutel, Garth; Moreno-Cruz, Juan, and Shayegh, Soheil. Climate tipping points and solar geoengineering. Journal of Economic Behavior & Organization, 132:19–45, 2016.

Heutel, Garth; Moreno-Cruz, Juan, and Shayegh, Soheil. Solar geoengineering, uncertainty, and the price of carbon. Journal of Environmental Economics and Management, 87:24–41, 2018.

Hoel, Michael and Karp, Larry. Taxes and quotas for a stock pollutant with multiplicative uncertainty. Journal of public Economics, 82(1):91–114, 2001.

Howard, Peter H and Sterner, Thomas. Few and not so far between: a meta-analysis of climate damage estimates. Environmental and Resource Economics, 68(1):197–225, 2017.

IPCC. Climate Change 2021: The Physical Science Basis. Contribution of Working Group I to the Sixth Assessment Report of the Intergovernmental Panel on Climate Change. Cambridge University Press, 2021.

Jones, Anthony C.; Hawcroft, Matthew K.; Haywood, James M.; Jones, Andy; Guo,

Xiaoran, and Moore, John C. Regional Climate Impacts of Stabilizing Global Warming at 1.5 K Using Solar Geoengineering. Earth's Future, 6(2):230–251, 2018.

Karp, Larry and Zhang, Jiangfeng. Regulation with anticipated learning about environmental damages. Journal of Environmental Economics and Management, 51(3): 259–279, 2006.

Keith, David W. and MacMartin, Douglas G. A temporary, moderate and responsive scenario for solar geoengineering. Nature Climate Change, 5(3):201–206, 2015.

Keith, David W.; Weisenstein, Debra K.; Dykema, John A., and Keutsch, Frank N. Stratospheric solar geoengineering without ozone loss. Proceedings of the National Academy of Sciences, 113(52):14910–14914, 2016.

Kelly, David L; Heutel, Garth; Moreno-Cruz, Juan B, and Shayegh, Soheil. Solar geoengineering, learning, and experimentation. Technical report, National Bureau of Economic Research, 2021.

Kleinschmitt, Christoph; Boucher, Olivier, and Platt, Ulrich. Sensitivity of the radiative forcing by stratospheric sulfur geoengineering to the amount and strategy of the SO2injection studied with the LMDZ-S3A model. Atmospheric Chemistry and Physics, 18(4):2769–2786, 2018.

Kravitz, Ben; Robock, Alan; Oman, Luke; Stenchikov, Georgiy, and Marquardt, Allison B. Sulfuric acid deposition from stratospheric geoengineering with sulfate aerosols. Journal of Geophysical Research Atmospheres, 114(14):1–7, 2009.

Kravitz, Ben; MacMartin, Douglas G.; Mills, Michael J.; Richter, Jadwiga H.; Tilmes, Simone; Lamarque, Jean-Francois; Tribbia, Joseph J., and Vitt, Francis. First simulations of designing stratospheric sulfate aerosol geoengineering to meet multiple simultaneous climate objectives. Journal of Geophysical Research: Atmospheres, 2017.

Lawrence, Mark G; Schäfer, Stefan; Muri, Helene; Scott, Vivian; Oschlies, Andreas; Vaughan, Naomi E; Boucher, Olivier; Schmidt, Hauke; Haywood, Jim, and Scheffran, Jürgen. Evaluating climate geoengineering proposals in the context of the Paris Agreement temperature goals. Nature Communications, 9(1):3734, 2018.

MacMartin, Douglas G.; Kravitz, Ben; Tilmes, Simone; Richter, Jadwiga H.; Mills, Michael J.; Lamarque, Jean-Francois; Tribbia, Joseph J., and Vitt, Francis. The climate response to stratospheric aerosol geoengineering can be tailored using multiple injection locations. Journal of Geophysical Research: Atmospheres, pages 574–590, 2017.

Manoussi, Vassiliki and Xepapadeas, Anastasios. Cooperation and competition in climate

change policies: mitigation and climate engineering when countries are asymmetric. Environmental and Resource Economics, 66(4):605–627, 2017.

Manoussi, Vassiliki; Xepapadeas, Anastasios, and Emmerling, Johannes. Climate engineering under deep uncertainty. Journal of Economic Dynamics and Control, 94: 207–224, 2018.

Meier, Felix D. and Traeger, Christian P. SolACE - solar geoengineering in an analytic climate economy. SSRN Working Paper 3958821, 2022. URL https://ssrn.com/abstract=3958821.

Moreno-Cruz, Juan B. and Keith, David W. Climate policy under uncertainty: A case for solar geoengineering. Climatic Change, 121(3):431–444, 2013.

Moreno-Cruz, Juan B; Ricke, Katharine L, and Keith, David W. A simple model to account for regional inequalities in the effectiveness of solar radiation management. Climatic Change, 110(3):649–668, 2012.

Newell, Richard G and Pizer, William A. Regulating stock externalities under uncertainty. Journal of environmental economics and management, 45(2):416–432, 2003.

Newell, Richard G; Prest, Brian C, and Sexton, Steven E. The gdp-temperature relationship: implications for climate change damages. Journal of Environmental Economics and Management, 108:102445, 2021.

Niemeier, U and Timmreck, C. What is the limit of climate engineering by stratospheric injection of SO2? Atmospheric Chemistry and Physics, 15(16):9129–9141, 2015.

Niemeier, Ulrike and Schmidt, Hauke. Changing transport processes in the stratosphere by radiative heating of sulfate aerosols. Atmospheric Chemistry and Physics, 17(24): 14871–14886, 2017.

Nordhaus, William. Climate change: The ultimate challenge for economics. American Economic Review, 109(6):1991–2014, 2019.

Nordhaus, William D and Boyer, Joseph. Warming the world: economic models of global warming. MIT press, 2000.

Nordhaus, William D and Sztorc, Paul. DICE2013R: Introduction and user's manual, 2013. URL http://www.econ.yale.edu/~nordhaus/homepage/homepage/documents/DICE_Manual_100413r1.pdf.

Roshan, Elnaz; M Khabbazan, Mohammad, and Held, Hermann. Cost-risk trade-off of mitigation and solar geoengineering: considering regional disparities under probabilistic climate sensitivity. Environmental and Resource Economics, 72(1):263–279, 2019.

Tallarini Jr, Thomas D. Risk-sensitive real business cycles. Journal of monetary Economics, 45(3):507–532, 2000.

Traeger, Christian P. ACE - Analytic Climate Economy (with Temperature and Uncertainty), 2018. URL `https://ssrn.com/abstract=3307622`.

Traeger, Christian P. Capturing intrinsic risk aversion. SSRN Working Paper 3462905, 2019.

Traeger, Christian P. ACE – Analytic Climate Economy. American Economic Journal: Economic Policy, 2021. forthcoming.

Traeger, Christian P. IAMs and CO_2 emissions – An analytic discussion. EAERE Working Paper, 2022.

Van den Bremer, Ton S and Van der Ploeg, Frederick. The risk-adjusted carbon price. American Economic Review, 111(9):2782–2810, 2021.

Visioni, Daniele; MacMartin, Douglas G.; Kravitz, Ben; Tilmes, Simone; Mills, Michael J.; Richter, Jadwiga H., and Boudreau, Matthew P. Seasonal Injection Strategies for Stratospheric Aerosol Geoengineering. Geophysical Research Letters, 46(13):7790–7799, 2019.

Visioni, Daniele; MacMartin, Douglas G; Kravitz, Ben; Boucher, Olivier; Jones, Andy; Lurton, Thibaut; Martine, Michou; Mills, Michael J; Nabat, Pierre; Niemeier, Ulrike, et al. Identifying the sources of uncertainty in climate model simulations of solar radiation modification with the g6sulfur and g6solar geoengineering model intercomparison project (geomip) simulations. Atmospheric Chemistry and Physics, 21(13): 10039–10063, 2021.

Weisenstein, D. K.; Keith, D. W., and Dykema, J. A. Solar geoengineering using solid aerosol in the stratosphere. Atmospheric Chemistry and Physics, 15(20):11835–11859, 2015.

Appendices

A Underlying Deterministic Model: Details

Production. Global gross output is a function of vectors of dimension I_j with $j \in \{A, N, K, E\}$ and the production function is stated in equation (1). Homogeneity of degree κ in capital is defined as

$$\mathcal{F}(\boldsymbol{A}_t,\, \lambda\, \boldsymbol{K}_t,\, \boldsymbol{N}_t,\, \boldsymbol{E}_t) = \lambda^{\kappa} \mathcal{F}(\boldsymbol{A}_t,\, \boldsymbol{K}_t,\, \boldsymbol{N}_t,\, \boldsymbol{E}_t) \quad \forall \quad \lambda \in \mathbb{R}_+. \tag{23}$$

Population size is normalized to unity $\sum_{i=1}^{I_N} N_{i,t} = 1$.[10]

Climate damages. Temperature-based damages are of the form

$$D_T(T_{1,t}) = \xi_0 \, \exp\left(\xi_1 \, T_{1,t}\right) - \xi_0, \tag{24}$$

see Traeger (2021) for a detailed discussion of the functional form and calibrations to various estimates in the literature.

Resource scarcity. The first I^d energy inputs $E_1, ..., E_{I^d}$ causing CO_2 emission are collected in the subvector $\boldsymbol{E}_t^d$. The vector $\boldsymbol{R}_t \in \mathbb{R}_+^{I^d}$ characterize fossil fuel resource stocks. The dynamics of the resource stock are

$$\boldsymbol{R}_{t+1} = \boldsymbol{R}_t - \boldsymbol{E}_t^d \tag{25}$$

with initial stock size $\boldsymbol{R}_0 \in \mathbb{R}_+^{I^d}$ given. Renewable energies are indexed by I^{d+1} to I_E. To avoid boundary value complications we assume that scarce resources are essential.

Carbon dioxide. Following DICE, we consider three carbon reservoirs, atmosphere (carbon content M_1), upper ocean (carbon content M_2) and lower ocean (carbon content M_3) which we summarize in the vector $\boldsymbol{M}$. An extension to additional carbon reservoirs is straight-forward. The dynamics of the carbon reservoirs is

$$\boldsymbol{M}_{t+1} = \boldsymbol{\Phi} \boldsymbol{M}_t + \tilde{\boldsymbol{e}}_t, \tag{26}$$

with the carbon cycle's transition matrix $\boldsymbol{\Phi}$. Further we define $\tilde{\boldsymbol{e}}_t = \boldsymbol{e}_1 \, E_t^{tot}$, with total

[10] We do not use population weighting in the objective function. The DICE model gives more weight to larger future population, in which case we could not normalize the population to unity. See Traeger (2021) for details.

CO_2 emissions $E_t^{tot} = \sum_{i=1}^{I^d} E_{i,t} + E_t^{\text{exo}}$ resulting from industrial fossil fuel burning and other exogenous processes including land use change and forestry. Similar to Traeger (2021), we define $\tilde{\phi} = [(\mathbf{1} - \beta\,\mathbf{\Phi})^{-1}]_{11}$. Instead of a simple decay, it captures how much carbon inserted into the atmosphere remains in or returns to the atmosphere over the discounted infinite time horizon.

Temperature dynamics. In the medium to long run a new level of radiative forcing implies the new atmospheric equilibrium temperature $T_{0,t} = \frac{s}{\eta} F_t$. Following ACE, we model the evolution of atmospheric temperature $T_{1,t}$ as a generalized mean of last period's atmospheric temperature (persistence), the last period's ocean temperature (currently cooling), and the new equilibrium temperature corresponding to radiative forcing $T_{0,t}$. Similarly ocean temperature $T_{2,t}$ evolves as a generalized mean of own past and atmospheric temperature

$$\begin{aligned} T_{1,t+1} &= \frac{1}{\xi_1} \log\Big((1 - \sigma^{forc} - \sigma_{21}) \exp(\xi_1\, T_{1,t}) + \sigma^{forc} \exp(\xi_1\, T_{0,t}) + \sigma_{21} \exp(\xi_1\, T_{2,t})\Big) \\ T_{2,t+1} &= \frac{1}{\xi_1} \log\Big((1 - \sigma_{12}) \exp(\xi_1\, T_{2,t}) + \sigma_{12} \exp(\xi_1\, T_{1,t})\Big) \end{aligned} \tag{27a}$$

with $\xi_1 = \frac{\log 2}{s}$. We rewrite these equations in terms of transformed temperatures $\tau_{it} = \exp(\xi_1\, T_{i,t})$ as

$$\begin{pmatrix} \tau_{1,t+1} \\ \tau_{2,t+1} \end{pmatrix} = \underbrace{\begin{pmatrix} 1 - \sigma_{\text{forc}} - \sigma_{21} & \sigma_{21} \\ \sigma_{12} & 1 - \sigma_{12} \end{pmatrix}}_{\equiv \boldsymbol{\sigma}} \begin{pmatrix} \tau_{1,t} \\ \tau_{2,t} \end{pmatrix} + \begin{pmatrix} \sigma_{\text{forc}} \exp\left(\frac{\log(2)}{\eta} F_t\right) \\ 0 \end{pmatrix}. \tag{27b}$$

Similar to Traeger (2021), we define

$$\tilde{\sigma} = \left[(\mathbf{1} - \beta\,\boldsymbol{\sigma})^{-1}\right]_{1,1}, \tag{28}$$

characterizing the discounted heat increase over the infinite time horizon resulting from a heat influx into the atmosphere in the present.

B Solving the Bellman equation: Long-run Uncertainty

Consumption rate and equations of motion under uncertainty. Solving the model

is simpler when controlling consumption in terms of the consumption rate

$$x_t = \frac{C_t}{Y_t\ [1 - D_t\,(T_{1,t}, S_t, m_t)]}. \tag{29}$$

where the geoengineering damges in equation (3) now takes on its stochastic form of equation (13).[11] Using the homogeneity of the production function

$$Y_t = \mathcal{F}(\boldsymbol{A}_t,\, \boldsymbol{K}_t,\, \boldsymbol{N}_t,\, \boldsymbol{E}_t) = K_t^{\kappa}\mathcal{F}(\boldsymbol{A}_t,\, \boldsymbol{\mathcal{K}}_t,\, \boldsymbol{N}_t,\, \boldsymbol{E}_t), \tag{30}$$

we transform the utility from consumption as

$$\log C_t = \log x_t + \kappa \log K_t + \log \mathcal{F}(\boldsymbol{A}_t,\, \boldsymbol{\mathcal{K}}_t,\, \boldsymbol{N}_t,\, \boldsymbol{E}_t) + \xi_0\ (1 - \tau_{1,t}) - d\, S_t + \pi_t^d - a(m_t - 1). \tag{31}$$

Defining log-capital as $k_t = \log K_t$, the equation of motion for capital is

$$k_{t+1} = \kappa\, k_t + \log \mathcal{F}(\boldsymbol{A}_t,\, \boldsymbol{\mathcal{K}}_t,\, \boldsymbol{N}_t,\, \boldsymbol{E}_t) + \log(1 - x_t) + \xi_0\ (1 - \tau_{1,t}) - d\, S_t + \pi_t^d - a(m_t - 1). \tag{32}$$

Including long-run uncertainty, the radiative forcing equation (15) is

$$F_t(m_t, S_t) = \frac{\eta}{\log(2)}\ \log\ \left(f_0 + f_1\, m_t + \left(f_2 - f_3\ \left(\frac{m_t}{S_t}\right)^n\right) S_t + \pi_t^{fl} + \pi_t^{fn}\right). \tag{33}$$

bringing the equation of motion (27b) for temperature

$$\boldsymbol{\tau}_{t+1} = \boldsymbol{\sigma}\boldsymbol{\tau}_t + \sigma_{\text{forc}} \exp\left(\frac{\log(2)}{\eta}\, F_t\right) \boldsymbol{e}_1$$

to the form

$$\boldsymbol{\tau}_{t+1} = \boldsymbol{\sigma}\boldsymbol{\tau}_t + \sigma_{\text{forc}}\Big(f_0 + f_1\, m_t + \Big(f_2 - f_3\ \Big(\frac{m_t}{S_t^{unc}}\Big)^n\Big) S_t^{unc} + \pi_t^{fl} + \pi_t^{fn}\Big)\boldsymbol{e}_1 \tag{34}$$

The new states capturing the persistence of the stochastic realizations π_{t+1}^d, π_{t+1}^{fl}, and π_{t+1}^{fn}

[11] We note that π_t^d is known at the time of consumption choice.

follow the equations (14), (16), and (19)

$$\pi^d_{t+1} = \epsilon^d_t \sqrt{S_t} + \Gamma^d \, \pi^d_t; \quad \pi^{fl}_{t+1} = \epsilon^{fl}_t \sqrt{S_t} + \Gamma^{fl} \, \pi^{fl}_t; \quad \pi^{fn}_{t+1} = \epsilon^{fn}_t \sqrt{\left(\frac{m_t}{S_t}\right)^n S_t} + \Gamma^{fn} \, \pi^{fn}_t \tag{35}$$

Bellman equation. We solve for the optimal policy using dynamic programming. The Bellman equation is

$$\begin{aligned} V(k_t, \boldsymbol{\tau}_t, \boldsymbol{M}_t, \boldsymbol{R}_t, \pi^d_t, \pi^{fl}_t, \pi^{fn}_t, t) = \max_{x_t, \boldsymbol{N}_t, \boldsymbol{\mathcal{K}}_t, \boldsymbol{E}_t, S_t} \Bigg\{ & \log x_t + \kappa \, k_t + \log \mathcal{F}(\boldsymbol{A}_t, \, \boldsymbol{\mathcal{K}}_t, \, \boldsymbol{N}_t, \, \boldsymbol{E}_t) \\ & + \xi_0 \, (1 - \tau_{1,t}) - d \, S_t + \, \pi^d_t - a(m_t - 1) \\ & + \frac{\beta}{\alpha} \, \log\Big(\mathbb{E}_t \exp[\alpha \, V(k_{t+1}, \boldsymbol{\tau}_{t+1}, \boldsymbol{M}_{t+1}, \boldsymbol{R}_{t+1}, \pi^d_{t+1}, \pi^{fl}_{t+1}, \pi^{fn}_{t+1}, t+1)] \Big) \Bigg\} \end{aligned} \tag{36}$$

with $\boldsymbol{R}_{t+1}, \boldsymbol{M}_{t+1}, \boldsymbol{\tau}_{t+1}$, and k_{t+1}, π^d_{t+1}, π^{fl}_{t+1}, and π^{fn}_{t+1} following the equations of motion (25), (26), (27b), and (32), (14), (16), and (19). We guess the following linear affine value function

$$\begin{aligned} & V(k_t, \boldsymbol{\tau}_t, \boldsymbol{M}_t, \boldsymbol{R}_t, \pi^d_t, \pi^{fl}_t, \pi^{fn}_t, t) = \\ & \quad \varphi_k \, k_t + \boldsymbol{\varphi}^T_\tau \, \boldsymbol{\tau}_t + \boldsymbol{\varphi}^T_M \, \boldsymbol{M}_t + \boldsymbol{\varphi}^T_{R,t} \, \boldsymbol{R}_t + \varphi^d_\pi \, \pi^d_t + \varphi^{fl}_\pi \, \pi^{fl}_t + \varphi^{fn}_\pi \, \pi^{fn}_t + \varphi_t. \end{aligned}$$

and will confirm our guess later on. Using this value function, we obtain the Bellman

equation

$$
\begin{aligned}
&\varphi_k\, k_t + \boldsymbol{\varphi}_\tau^T\, \boldsymbol{\tau}_t + \boldsymbol{\varphi}_M^T\, \boldsymbol{M}_t + \boldsymbol{\varphi}_{R,t}^T\, \boldsymbol{R}_t + \varphi_\pi^d\, \pi_t^d + \varphi_\pi^{fl}\, \pi_t^{fl} + \varphi_\pi^{fn}\, \pi_t^{fn} + \varphi_t \\
&= \max_{x_t, \boldsymbol{N}_t, \boldsymbol{\mathcal{K}}_t, \boldsymbol{E}_t, S_t} \Bigg\{ \log x_t + \kappa\, k_t + \log \mathcal{F}(\boldsymbol{A}_t,\, \boldsymbol{\mathcal{K}}_t,\, \boldsymbol{N}_t,\, \boldsymbol{E}_t) + \xi_0\, (1 - \tau_{1,t}) - d\, S_t - a(m_t - 1) \\
&\qquad + \underbrace{\pi_t^d}_{utility} + \lambda_t^{\mathcal{K}}(1 - \sum_{i=1}^{I_K} \mathcal{K}_{i,t}) + \lambda_t^N(1 - \sum_{i=1}^{I_N} N_{i,t}) \\
&\qquad + \beta\, \varphi_k \Big(\kappa\, k_t + \log \mathcal{F}(\boldsymbol{A}_t,\, \boldsymbol{\mathcal{K}}_t,\, \boldsymbol{N}_t,\, \boldsymbol{E}_t) + \log(1 - x_t) + \xi_0\, (1 - \tau_{1,t}) \\
&\qquad\qquad - d\, S_t - a(m_t - 1) \Big) \\
&\qquad + \beta\, \boldsymbol{\varphi}_\tau^T \Big(\boldsymbol{\sigma}\boldsymbol{\tau}_t + \sigma_{\text{forc}} \Big(f_0 + f_1\, m_t + \Big(f_2 - f_3 \Big(\frac{m_t}{S_t} \Big)^n \Big) S_t \Big) \boldsymbol{e}_1 \Big) \\
&\qquad + \beta\, \boldsymbol{\varphi}_M^T\, (\boldsymbol{\Phi}\boldsymbol{M}_t + \tilde{\boldsymbol{e}}_{\boldsymbol{t}}) + \beta\, \boldsymbol{\varphi}_{R,t+1}^T\, \left(\boldsymbol{R}_t - \boldsymbol{E}_t^d \right) + \beta\, \varphi_{t+1} \\
&\qquad + \frac{\beta}{\alpha}\, \log \Big(\mathbb{E}_t \exp \big[\alpha \big(\underbrace{\varphi_\pi^d\, \epsilon_t^d \sqrt{S_t} + \varphi_\pi^d\, \Gamma^d\, \pi_t^d}_{\pi_{t+1}^d} + \underbrace{\varphi_k\, \pi_t^d}_{k_{t+1}} \big) \big] \Big) \\
&\qquad + \frac{\beta}{\alpha}\, \log \Big(\mathbb{E}_t \exp \big[\alpha \big(\underbrace{\varphi_\pi^{fl}\, \epsilon_t^{fl} \sqrt{S_t} + \varphi_\pi^{fl}\, \Gamma^{fl}\, \pi_t^{fl}}_{\pi_{t+1}^{fl}} + \underbrace{\varphi_{\tau 1}\, \sigma_{\text{forc}}\, \pi_t^{fl}}_{\tau_{t+1}} \big) \big] \Big) \\
&\qquad + \frac{\beta}{\alpha}\, \log \Big(\mathbb{E}_t \exp \big[\alpha \big(\underbrace{\varphi_\pi^{fn}\, \epsilon_t^{fn} \sqrt{\Big(\frac{m_t}{S_t} \Big)^n S_t} + \varphi_\pi^{fn}\, \Gamma^{fn}\, \pi_t^{fn}}_{\pi_{t+1}^{fn}} \\
&\qquad\qquad + \underbrace{\varphi_{\tau 1}\, \sigma_{\text{forc}}\, \pi_t^{fn}}_{\tau_{t+1}} \big) \big] \Big) \Bigg\}.
\end{aligned}
$$

The argument of the expected value operator on the r.h.s. of the Bellman equation contains both normally distributed components and determinsitic components, all of which appear in the exponential. Conditional on information in period t, all period t states are known and only those terms depending on the ϵ-shocks are stochastic. Deterministic terms can simply be pulled through the log-exp concatination (and the risk aversion parameter α cancels). To evaluate the stochastic terms, we note that $\mathcal{M}(z) = \mathbb{E}_t \exp(z\epsilon)$ defines the moment generating function of the stochastic variable ϵ. In our case $\epsilon \sim \mathcal{N}(0,\, \sigma^2)$ and the moment generating function of the normal distribution is $\mathcal{M}(z) = \exp(\mu z + \frac{\sigma^2}{2} z^2)$, where in our case $\mu = 0$. Then, the stochastic components of the Bellman equation are

of the form

$$\frac{\beta}{\alpha}\,\log\big(\,\mathbb{E}_t\exp(\alpha\bar{z}\epsilon)\big)=\beta\alpha\frac{\sigma^2}{2}\bar{z}^2$$

where $\bar{z}$ stands for the terms accompanying ϵ^d, ϵ^{fl}, or ϵ^{fl} respectively. Evaluating the damage and forcing uncertainties and simplifying yields

$$\begin{aligned}
&\varphi_k\,k_t+\boldsymbol{\varphi}_\tau^T\,\boldsymbol{\tau}_t+\;\boldsymbol{\varphi}_M^T\,\boldsymbol{M}_t+\boldsymbol{\varphi}_{R,t}^T\,\boldsymbol{R}_t+\varphi_\pi^d\,\pi_t^d+\varphi_\pi^{fl}\,\pi_t^{fl}+\varphi_\pi^{fn}\,\pi_t^{fn}+\varphi_t\\
&=\max_{x_t,\boldsymbol{N}_t,\boldsymbol{\mathcal{K}}_t,\boldsymbol{E}_t,S_t}\Bigg\{\log x_t+\kappa\,k_t+\log\mathcal{F}(\boldsymbol{A}_t,\,\boldsymbol{\mathcal{K}}_t,\,\boldsymbol{N}_t,\,\boldsymbol{E}_t)+\xi_0\;(1-\tau_{1,t})-d\,S_t-a(m_t-1)\\
&\qquad+\lambda_t^{\mathcal{K}}(1-\sum_{i=1}^{I_K}\mathcal{K}_{i,t})+\lambda_t^{N}(1-\sum_{i=1}^{I_N}N_{i,t})\\
&\qquad+\beta\,\varphi_k\,\Big(\kappa\,k_t+\log\mathcal{F}(\boldsymbol{A}_t,\,\boldsymbol{\mathcal{K}}_t,\,\boldsymbol{N}_t,\,\boldsymbol{E}_t)+\log(1-x_t)+\xi_0\;(1-\tau_{1,t})\\
&\qquad\qquad-d\,S_t-a(m_t-1)\Big)\\
&\qquad+\beta\,\boldsymbol{\varphi}_\tau^T\,\Big(\boldsymbol{\sigma}\boldsymbol{\tau}_t+\sigma_{\text{forc}}\Big(f_0+f_1\,m_t+\Big(f_2-f_3\Big(\frac{m_t}{S_t}\Big)^n\Big)S_t\Big)\boldsymbol{e}_1\Big)\\
&\qquad+\beta\,\boldsymbol{\varphi}_M^T\;(\boldsymbol{\Phi}\boldsymbol{M}_t+\tilde{\boldsymbol{e}}_{\boldsymbol{t}})+\beta\,\boldsymbol{\varphi}_{R,t+1}^T\;\big(\boldsymbol{R}_t-\boldsymbol{E}_t^d\big)+\beta\,\varphi_{t+1}\\
&\qquad+\alpha\,\beta^{\,2}(\varphi_\pi^d)^2\frac{(\sigma^d)^2}{2}S_t+\big((1+\beta\,\varphi_k)+\beta\,\varphi_\pi^d\,\Gamma^d\big)\;\pi_t^d\\
&\qquad+\alpha\,\beta\,(\varphi_\pi^{fl})^2\frac{(\sigma^{fl})^2}{2}S_t+(\varphi_{\tau 1}\,\sigma_{\text{forc}}+\varphi_\pi^{fl}\,\Gamma^{fl})\beta\;\pi_t^{fl}\Bigg\}.\\
&\qquad+\alpha\,\beta\,(\varphi_\pi^{fn})^2\frac{(\sigma^{fn})^2}{2}\Big(\frac{m_t}{S_t}\Big)^n S_t+(\varphi_{\tau 1}\,\sigma_{\text{forc}}+\varphi_\pi^{fn}\,\Gamma^{fn})\beta\;\pi_t^{fn}\Bigg\}.
\end{aligned}\tag{37}$$

To get equation (37) we calculate

$$\begin{aligned}
(i)\;&\underbrace{\pi_t^d}_{utility}+\frac{\beta}{\alpha}\,\log\Big(\mathbb{E}_t\exp\big[\alpha\big(\underbrace{\varphi_\pi^d\,\epsilon_t^d\sqrt{S_t}+\varphi_\pi^d\Gamma^d\,\pi_t^d}_{\pi_{t+1}^d}+\underbrace{\varphi_k\,\pi_t^d}_{k_{t+1}}\big)\big]\Big)\\
&=\frac{\beta}{\alpha}\alpha^{22}(\varphi_\pi^d)^2\frac{(\sigma^d)^2}{2}S_t+(1+\beta\varphi_k)\pi_t^d+\beta\varphi_\pi^d\Gamma^d\pi_t^d\\
&=\alpha\beta^2(\varphi_\pi^d)^2\frac{(\sigma^d)^2}{2}S_t+\big((1+\beta\varphi_k)+\beta\varphi_\pi^d\Gamma^d\big)\,\pi_t^d
\end{aligned}$$

$$
\begin{aligned}
(ii)\quad & \frac{\beta}{\alpha}\,\log\Big(\mathbb{E}_t \exp\big[\alpha\big(\underbrace{\varphi_\pi^{fl}\,\epsilon_t^{fl}\sqrt{S_t} + \varphi_\pi^{fl}\;\Gamma^{fl}\,\pi_t^{fl}}_{\pi_{t+1}^{fl}} + \underbrace{\varphi_{\tau 1}\,\sigma_{\text{forc}}\;\pi_t^{fl}}_{\tau_{t+1}}\big)\big]\Big) \\
& = \frac{\beta}{\alpha}\alpha^2(\varphi_\pi^{fl})^2\frac{(\sigma^{fl})^2}{2}S_t + \beta\,\varphi_{\tau 1}\sigma_{\text{forc}}\;\pi_t^{fl} + \beta\,\varphi_\pi^{fl}\;\Gamma^{fl}\,\pi_t^{fl} \\
& = \alpha\,\beta(\varphi_\pi^{fl})^2\frac{(\sigma^{fl})^2}{2}S_t + (\varphi_{\tau 1}\,\sigma_{\text{forc}} + \varphi_\pi^{fl}\,\Gamma^{fl})\beta\;\pi_t^{fl}
\end{aligned}
$$

(iii) and the analoguous calculation for π^{fn}.

First order conditions. Maximizing the right hand side over x_t yields

$$
\frac{1}{x_t} - \beta\,\varphi_k\frac{1}{1-x_t} = 0 \quad \Longrightarrow \quad x_t = \frac{1}{1+\beta\,\varphi_k}. \tag{38}
$$

Maximizing the right hand side over $\mathcal{K}_{i,t}$ yields

$$
(1+\beta\,\varphi_k)\frac{\frac{\partial \mathcal{F}(\boldsymbol{A}_t,\boldsymbol{\mathcal{K}}_t,\boldsymbol{N}_t,\boldsymbol{E}_t)}{\partial \mathcal{K}_{i,t}}}{\mathcal{F}(\boldsymbol{A}_t,\,\boldsymbol{\mathcal{K}}_t,\,\boldsymbol{N}_t,\,\boldsymbol{E}_t)} = \lambda_t^{\mathcal{K}}
$$

which is equivalent to

$$
\mathcal{K}_{i,t} = \frac{\sigma_{Y,\mathcal{K}_i}(\boldsymbol{A}_t,\,\boldsymbol{\mathcal{K}}_t,\,\boldsymbol{N}_t,\,\boldsymbol{E}_t)}{\sum_{i=1}^{I_K}\sigma_{Y,\mathcal{K}_i}(\boldsymbol{A}_t,\,\boldsymbol{\mathcal{K}}_t,\,\boldsymbol{N}_t,\,\boldsymbol{E}_t)} \tag{39}
$$

with

$$
\sigma_{Y,\mathcal{K}_i}(\boldsymbol{A}_t,\,\boldsymbol{\mathcal{K}}_t,\,\boldsymbol{N}_t,\,\boldsymbol{E}_t) \equiv \frac{\partial \mathcal{F}(\boldsymbol{A}_t,\,\boldsymbol{\mathcal{K}}_t,\,\boldsymbol{N}_t,\,\boldsymbol{E}_t)}{\partial \mathcal{K}_{i,t}}\frac{\mathcal{K}_{i,t}}{\mathcal{F}(\boldsymbol{A}_t,\,\boldsymbol{\mathcal{K}}_t,\,\boldsymbol{N}_t,\,\boldsymbol{E}_t)}.
$$

Similarly, the first order conditions for the labor input is

$$
(1+\beta\,\varphi_k)\frac{\frac{\partial \mathcal{F}(\boldsymbol{A}_t,\boldsymbol{\mathcal{K}}_t,\boldsymbol{N}_t,\boldsymbol{E}_t)}{\partial N_{i,t}}}{\mathcal{F}(\boldsymbol{A}_t,\,\boldsymbol{\mathcal{K}}_t,\,\boldsymbol{N}_t,\,\boldsymbol{E}_t)} = \lambda_t^{N}
$$

and hence

$$N_{i,t} = \frac{\sigma_{Y,N_i}(\boldsymbol{A}_t,\, \boldsymbol{\mathcal{K}}_t,\, \boldsymbol{N}_t,\, \boldsymbol{E}_t)}{\sum_{i=1}^{I_N} \sigma_{Y,N_i}(\boldsymbol{A}_t,\, \boldsymbol{\mathcal{K}}_t,\, \boldsymbol{N}_t,\, \boldsymbol{E}_t)} \tag{40}$$

with

$$\sigma_{Y,N_i}(\boldsymbol{A}_t,\, \boldsymbol{\mathcal{K}}_t,\, \boldsymbol{N}_t,\, \boldsymbol{E}_t) \equiv \frac{\partial \mathcal{F}(\boldsymbol{A}_t,\, \boldsymbol{\mathcal{K}}_t,\, \boldsymbol{N}_t,\, \boldsymbol{E}_t)}{\partial N_{i,t}} \frac{N_{i,t}}{\mathcal{F}(\boldsymbol{A}_t,\, \boldsymbol{\mathcal{K}}_t,\, \boldsymbol{N}_t,\, \boldsymbol{E}_t)}$$

The first order condition for the optimal input of fossil fuels is given by

$$(1+\beta\,\varphi_k)\frac{\frac{\partial \mathcal{F}(\boldsymbol{A}_t, \boldsymbol{\mathcal{K}}_t, \boldsymbol{N}_t, \boldsymbol{E}_t)}{\partial E_{i,t}}}{\mathcal{F}(\boldsymbol{A}_t,\, \boldsymbol{\mathcal{K}}_t,\, \boldsymbol{N}_t,\, \boldsymbol{E}_t)} = \beta(\varphi_{R,i,t+1} - \varphi_{M1})$$

which is equivalent to

$$E_{i,t} = \frac{(1+\beta\,\varphi_k)\sigma_{Y,E_i}(\boldsymbol{A}_t,\, \boldsymbol{\mathcal{K}}_t,\, \boldsymbol{N}_t,\, \boldsymbol{E}_t)}{\beta(\varphi_{R,i,t+1} - \varphi_{M1})} \tag{41}$$

with

$$\sigma_{Y,E_i}(\boldsymbol{A}_t,\, \boldsymbol{\mathcal{K}}_t,\, \boldsymbol{N}_t,\, \boldsymbol{E}_t) \equiv \frac{\partial \mathcal{F}(\boldsymbol{A}_t,\, \boldsymbol{\mathcal{K}}_t,\, \boldsymbol{N}_t,\, \boldsymbol{E}_t)}{\partial E_{i,t}} \frac{E_{i,t}}{\mathcal{F}(\boldsymbol{A}_t,\, \boldsymbol{\mathcal{K}}_t,\, \boldsymbol{N}_t,\, \boldsymbol{E}_t)}.$$

Spelling out the part of the Bellman equation (37) that depends on sulfur we find

$$\begin{aligned} B_t^S = {} & \beta\,\varphi_{\tau 1}\,\sigma_{\text{forc}}\,f_2\,S_t - \beta\,\varphi_{\tau 1}\,\sigma_{\text{forc}} f_3\,m_t^n\,S_t^{(1-n)} - (1+\beta\,\varphi_k)\,d\,S_t + \alpha\,\beta^{\,2}(\varphi_\pi^d)^2\,\frac{(\sigma^d)^2}{2}\,S_t \\ & + \alpha\,\beta\;(\varphi_\pi^{fl})^2\,\frac{(\sigma^{fl})^2}{2}\,S_t + \alpha\,\beta\,(\varphi_\pi^{fn})^2\frac{(\sigma^{fn})^2}{2}\,m_t^n\,S_t^{(1-n)}. \end{aligned} \tag{42}$$

The first order condition for optimal sulfur deployment then results in[12]

$$\begin{aligned} & \beta\,\varphi_{\tau 1}\,\sigma_{\text{forc}} f_2 + \beta\,\varphi_{\tau 1}\,\sigma_{\text{forc}}(n-1) f_3\,m_t^n\,S_t^{-n}) - (1+\beta\,\varphi_k)\,d + \alpha\,\beta^{\,2}(\varphi_\pi^d)^2\,\frac{(\sigma^d)^2}{2} \\ & + \alpha\,\beta\,(\varphi_\pi^{fl})^2\,\frac{(\sigma^{fl})^2}{2} + (1-n)\alpha\,\beta\,(\varphi_\pi^{fn})^2\frac{(\sigma^{fn})^2}{2}\,m_t^n\,S_t^{-n} = 0. \end{aligned}$$

[12]The second derivative gives $-n\,\beta\,\varphi_{\tau 1}\,\sigma_{\text{forc}}(n-1) f_3\,m_t^n\,S_t^{-(1+n)} < 0$ so that the condition indeed identifies the maximal value deriving from sulfur deployment in a given period.

Solving for S_t leads to

$$S_t^{unc} = \underbrace{\left(\frac{(1-n)\left(-\beta\,\varphi_{\tau 1}\,\sigma_{\text{forc}}\,f_3 + \alpha\,\beta\,(\varphi_\pi^{fn})^2\frac{(\sigma^{fn})^2}{2}\right)}{(1+\beta\,\varphi_k)\,d - \beta\,\varphi_{\tau 1}\,\sigma_{\text{forc}} f_2 - \alpha\,\beta^{\,2}(\varphi_\pi^d)^2\frac{(\sigma^d)^2}{2} - \alpha\,\beta\,(\varphi_\pi^{fl})^2\frac{(\sigma^{fl})^2}{2}} \right)^{\frac{1}{n}}}_{\equiv z^{unc}} m_t \quad (43)$$

Solving the system of first order conditions gives us $\boldsymbol{N}_t^*(\boldsymbol{A}_t, \varphi_k, \boldsymbol{\varphi}_M, \boldsymbol{\varphi}_{R,t+1})$, $\boldsymbol{\mathcal{K}}_t^*(\boldsymbol{A}_t, \varphi_k, \boldsymbol{\varphi}_M, \boldsymbol{\varphi}_{R,t+1})$, and $\boldsymbol{E}_t^*(\boldsymbol{A}_t, \varphi_k, \boldsymbol{\varphi}_M, \boldsymbol{\varphi}_{R,t+1})$ which are independent of the states and $S_t^{unc}(\varphi_k, \varphi_{\tau 1}, \varphi_\pi^d, \varphi_\pi^{fl}, M_{1,t})$ which depends on the atmospheric carbon stock. In the following we show that given these optimal controls the maximized Bellman equation is linear in all states.

Shadow values. Inserting the optimal control rules into the maximized Bellman equation gives us

$$\begin{aligned}
&\varphi_k\,k_t\; + \boldsymbol{\varphi}_\tau^T\,\boldsymbol{\tau}_t + \boldsymbol{\varphi}_M^T\,\boldsymbol{M}_t + \boldsymbol{\varphi}_{R,t}^T\,\boldsymbol{R}_t + \varphi_\pi^d\,\pi_t^d + \varphi_\pi^{fl}\,\pi_t^{fl} + \varphi_t \\
= \quad & \log x_t^* + \kappa\,k_t + \log\mathcal{F}(\boldsymbol{A}_t,\,\boldsymbol{\mathcal{K}}_t^*,\,\boldsymbol{N}_t^*,\,\boldsymbol{E}_t^*) + \xi_0\,(1-\tau_{1,t}) - d\,S_t^{unc} - a(m_t-1) \\
& + \beta\,\varphi_k\left(\kappa\,k_t + \log\mathcal{F}(\boldsymbol{A}_t,\,\boldsymbol{\mathcal{K}}_t^*,\,\boldsymbol{N}_t^*,\,\boldsymbol{E}_t^*) + \log(1-x_t^*) + \xi_0\,(1-\tau_{1,t}) - d\,S_t^{unc} - a(m_t-1)\right) \\
& + \beta\,\boldsymbol{\varphi}_\tau^T\left(\boldsymbol{\sigma}\boldsymbol{\tau}_t + \sigma_{\text{forc}}\Big(f_0 + f_1\,m_t + \Big(f_2 - f_3\left(\frac{m_t}{S_t^{unc}}\right)^n\Big)S_t^{unc}\Big)\boldsymbol{e}_1\right) \\
& + \beta\,\boldsymbol{\varphi}_M^T\,(\boldsymbol{\Phi}\boldsymbol{M}_t + \tilde{\boldsymbol{e}}_{\boldsymbol{t}}) + \beta\,\boldsymbol{\varphi}_{R,t+1}^T\left(\boldsymbol{R}_t - \boldsymbol{E}_t^{d*}\right) + \beta\,\varphi_{t+1} \\
& + \alpha\beta^2(\varphi_\pi^d)^2\frac{(\sigma^d)^2}{2}S_t^{unc} + \left((1+\beta\varphi_k) + \beta\varphi_\pi^d\Gamma^d\right)\,\pi_t^d \\
& + \alpha\beta^2(\varphi_\pi^{fl})^2\frac{(\sigma^{fl})^2}{2}S_t^{unc} + (\varphi_{\tau 1}\,\sigma_{\text{forc}} + \varphi_\pi^{fl}\Gamma^{fl})\beta\,\pi_t^{fl} \\
& + \alpha\,\beta\,(\varphi_\pi^{fn})^2\frac{(\sigma^{fn})^2}{2}\,m_t^n\,S_t^{unc(1-n)} + (\varphi_{\tau 1}\,\sigma_{\text{forc}} + \varphi_\pi^{fn}\,\Gamma^{fn})\beta\,\pi_t^{fn}
\end{aligned}$$

Arranging terms with respect to their states and using the propensity definition z^{unc} yields

$$
\begin{aligned}
&\varphi_k\, k_t \; + \boldsymbol{\varphi}_\tau^T\, \boldsymbol{\tau}_t + \boldsymbol{\varphi}_M^T\, \boldsymbol{M}_t + \boldsymbol{\varphi}_{R,t}^T\, \boldsymbol{R}_t + \varphi_\pi^d\, \pi_t^d + \varphi_\pi^{fl}\, \pi_t^{fl} + \varphi_\pi^{fn}\, \pi_t^{fn} + \varphi_t \\
= \quad & \Big[(1+\beta\,\varphi_k)\kappa\Big] k_t + \Big[\beta\, \boldsymbol{\varphi}_\tau^T\, \boldsymbol{\sigma} - (1+\beta\,\varphi_k)\xi_0\, \boldsymbol{e}_1^T\Big] \boldsymbol{\tau}_t \\
& + \Big[\beta\, \boldsymbol{\Phi} \boldsymbol{\varphi}_M^T + \Big((\beta\,\varphi_{\tau 1}\,\sigma_{\text{forc}})\Big(f_1 + f_2\, z^{unc} - f_3\,(z^{unc})^{1-n}\Big) + \alpha\,\beta^{\,2} (\varphi_\pi^d)^2 \frac{(\sigma^d)^2}{2}\, z^{unc} \\
& \qquad + \alpha\,\beta\,(\varphi_\pi^{fl})^2 \frac{(\sigma^{fl})^2}{2}\, z^{unc} + \alpha\,\beta\,(\varphi_\pi^{fn})^2 \frac{(\sigma^{fn})^2}{2}\,(z^{unc})^{1-n} \\
& - (1+\beta\,\varphi_k)(a + d\, z^{unc})\Big) M_{pre}^{-1}\, \boldsymbol{e}_1^T\Big] \boldsymbol{M}_t + \Big[\,\Big((1+\beta\,\varphi_k) + \beta\,\varphi_\pi^d\,\Gamma^d\Big)\,\Big] \pi_t^d \\
& + \Big[(\varphi_{\tau 1}\,\sigma_{\text{forc}} + \varphi_\pi^{fl}\,\Gamma^{fl})\beta\,\Big] \pi_t^{fl} + \Big[(\varphi_{\tau 1}\,\sigma_{\text{forc}} + \varphi_\pi^{fn}\,\Gamma^{fn})\beta\,\Big] \pi_t^{fn} + \Big[\beta\, \boldsymbol{\varphi}_{R,t+1}^T\Big] R_t \\
& + \log\, x_t^* + \beta\,\varphi_k\, \log(1 - x_t^*) + (1+\beta\,\varphi_k) \log \mathcal{F}(\boldsymbol{A}_t,\, \boldsymbol{\mathcal{K}}_t^*,\, \boldsymbol{N}_t^*,\, \boldsymbol{E}_t^*) \\
& + (1+\beta\,\varphi_k)(\xi_0 + a) + \beta\,\varphi_{\tau 1}\,\sigma_{\text{forc}}\, f_0 + \beta\, \boldsymbol{\varphi}_M^T\, \tilde{\boldsymbol{e}}_t - \beta\, \boldsymbol{\varphi}_{R,t+1}^T\, \boldsymbol{E}_t^{d*} + \beta\,\varphi_{t+1}. \qquad (44)
\end{aligned}
$$

Matching the coefficients of the new state π_t^d on the r.h.s. Bellman equation (see above) with the term $\varphi_\pi^d \pi_t^d$ on the l.h.s. Bellman equation delivers

$$
\begin{aligned}
& \varphi_\pi^d = \Big((1+\beta\,\varphi_k) + \beta\,\varphi_\pi\,\Gamma^d\Big) \\
& \Leftrightarrow (1 - \beta\,\Gamma^d)\varphi_\pi^d = (1+\beta\,\varphi_k) \\
& \Leftrightarrow \varphi_\pi^d = \frac{1+\beta\,\varphi_k}{1-\beta\;\Gamma^d}
\end{aligned}
$$

and similarly for the state π_t^{fl}

$$
\begin{aligned}
& \varphi_\pi^{fl} = (\varphi_{\tau 1}\,\sigma_{\text{forc}} + \varphi_\pi^{fl}\,\Gamma^{fl})\beta \\
& \Leftrightarrow (1 - \Gamma^{fl}\,\beta\,)\varphi_\pi^{fl} = \varphi_{\tau 1}\,\sigma_{\text{forc}}\,\beta \\
& \Leftrightarrow \varphi_\pi^{fl} = \frac{\varphi_{\tau 1}\,\sigma_{\text{forc}}\,\beta}{1-\beta\;\Gamma^{fl}}
\end{aligned}
$$

and for the state φ_π^{fn}

$$
\begin{aligned}
& \varphi_\pi^{fn} = (\varphi_{\tau 1}\,\sigma_{\text{forc}} + \varphi_\pi^{fn}\,\Gamma^{fn})\beta \\
& \Leftrightarrow (1 - \Gamma^{fn}\,\beta\,)\varphi_\pi^{fn} = \varphi_{\tau 1}\,\sigma_{\text{forc}}\,\beta \\
& \Leftrightarrow \varphi_\pi^{fn} = \frac{\varphi_{\tau 1}\,\sigma_{\text{forc}}\,\beta}{1-\beta\;\Gamma^{fn}}
\end{aligned}
$$

Coefficient matching for capital leads to

$$\varphi_k = (1 + \beta\,\varphi_k)\kappa \quad \Leftrightarrow \quad \varphi_k = \frac{\kappa}{1 - \beta\,\kappa} \tag{45}$$

Coefficient matching with respect to transformed temperatures delivers

$$\boldsymbol{\varphi}_\tau^T = -\xi_0\,(1 + \beta\,\varphi_k)\,\boldsymbol{e}_1^T\,(\mathbf{1} - \beta\,\boldsymbol{\sigma})^{-1}.$$

where we denote the entries of the inverted matrix as follows

$$\begin{pmatrix} \tilde{\sigma}_{11} & \tilde{\sigma}_{12} \\ \tilde{\sigma}_{21} & \tilde{\sigma}_{22} \end{pmatrix} \equiv (\mathbf{1} - \beta\,\boldsymbol{\sigma})^{-1}$$

yielding

$$\tilde{\sigma}_{11} = \left[(\mathbf{1} - \beta\,\boldsymbol{\sigma})^{-1}\right]_{1,1} \tag{46}$$

where $[\cdot]_{1,1}$ denotes the first element of the inverted matrix in square brackets. Thus, using φ_k from equation (45) transformed atmospheric temperature is given by

$$\begin{aligned} \varphi_{\tau 1} &= -\xi_0\,(1 + \beta\,\varphi_k)\tilde{\sigma}_{11} \\ &= -\frac{\xi_0}{1 - \beta\,\kappa}\tilde{\sigma}_{11} \end{aligned} \tag{47}$$

Using the solutions for φ_k and $\varphi_{\tau 1}$ in φ_π^d, φ_π^{fl} and φ_π^{fn} leads to

$$\varphi_\pi^d = \frac{}{(1 - \beta\,\kappa)(1 - \beta\;\Gamma^d)} \tag{48}$$

$$\varphi_\pi^{fl} = -\frac{\xi_0\,\tilde{\sigma}_{11}\,\sigma_{\text{forc}}\,\beta}{(1 - \beta\,\kappa)(1 - \beta\;\Gamma^{fl})} \tag{49}$$

$$\varphi_\pi^{fn} = -\frac{\xi_0\,\tilde{\sigma}_{11}\,\sigma_{\text{forc}}\,\beta}{(1 - \beta\,\kappa)(1 - \beta\;\Gamma^{fn})}$$

Coefficient matching with respect to the atmospheric carbon stock yields

$$\boldsymbol{\varphi}_M^\top = \Big((\beta\,\varphi_{\tau 1}\,\sigma_{\text{forc}}) \left(f_1 + f_2\,z - f_3\,z^{1-n}\right) + \alpha\,\beta^{\,2} (\varphi_\pi^d)^2 \frac{(\sigma^d)^2}{2}\, z^{unc} + \alpha\,\beta\,(\varphi_\pi^{fl})^2 \frac{(\sigma^{fl})^2}{2}\, z^{unc}$$
$$+\alpha\,\beta\,(\varphi_\pi^{fn})^2 \frac{(\sigma^{fn})^2}{2}\,(z^{unc})^{1-n} - (1+\beta\,\varphi_k)(a + d\,z)\Big) M_{pre}^{-1}\,\boldsymbol{e}_1^\top\,(\mathbf{1} - \beta\,\boldsymbol{\Phi})^{-1}. \tag{50}$$

We define

$$\tilde{\phi}_{ij} = \left[(\mathbf{1} - \beta\,\boldsymbol{\Phi})^{-1}\right]_{ij} \text{ for } i,j \in \{1,2,3\},$$

yielding

$$\tilde{\phi}_{11} = \left[(\mathbf{1} - \beta\,\boldsymbol{\Phi})^{-1}\right]_{1,1} \tag{51}$$

where $[\cdot]_{1,1}$ denotes the first element of the inverted matrix in square brackets. Note that for ease of representation we drop the subscript of the term $\tilde{\phi}_{11}$ and instead use $\tilde{\phi}$.

Coefficient matching with respect to the resource stock yields

$$\boldsymbol{\varphi}_{R,t}^T = \beta\,\boldsymbol{\varphi}_{R,t+1}^T \quad \Leftrightarrow \quad \boldsymbol{\varphi}_{R,t} = \beta^{-t}\boldsymbol{\varphi}_{R,0} \quad \text{(Hotelling's rule)}.$$

The initial resource values $\boldsymbol{\varphi}_{R,0}^T$ depend on the set up of the economy, including assumptions about production and the energy sector. Given the coefficients and the optimal rate of consumption equation (44) turns to the following condition:

$$\varphi_t - \beta\,\varphi_{t+1} = \log\,x_t^* + \beta\,\varphi_k\,\log(1-x_t^*) + (1+\beta\,\varphi_k)\log\mathcal{F}(\boldsymbol{A}_t,\,\boldsymbol{\mathcal{K}}_t^*,\,\boldsymbol{N}_t^*,\,\boldsymbol{E}_t^*)$$
$$+ (1+\beta\,\varphi_k)(\xi_0 + a) + \beta\,\varphi_{\tau 1}\,\sigma_{\text{forc}}\,f_0 + \beta\,\boldsymbol{\varphi}_M^T\,\tilde{\boldsymbol{e}}_t - \beta\,\boldsymbol{\varphi}_{R,t+1}^T\,\boldsymbol{E}_t^{d*} \tag{52}$$

This condition will be satisfied by picking the sequence $\varphi_0, \varphi_1, \varphi_2, ...$ The additional condition $\lim_{t\to\infty}\beta^t V(\cdot) = 0 \Rightarrow \lim_{t\to\infty}\beta^t\varphi_t = 0$ pins down this initial value φ_0.

Optimal level of sulfur. We insert (45), (47), (48) and (49) for the shadow values φ_k, $\varphi_{\tau 1}$, φ_π^d and φ_π^{fl} into our expression for optimal sulfur deployment (43). Note that for ease of representation we use the following definition, $\tilde{\sigma} = \tilde{\sigma}_{11}\,\sigma_{\text{forc}}$. Further, we define $\gamma = \beta\,\xi_0\,\tilde{\sigma}$, which delivers

$$S_t^{unc} = \left(\frac{(1-n)\,\gamma\, f_3 + \frac{\alpha\,\beta\,(1-n)}{(1-\beta\,\kappa)} \left[\overbrace{\frac{\gamma^{2\,4}}{(1-\beta\;\Gamma^{fn})^2}\,\frac{(\sigma^{fn})^2}{2}}^{\text{forcing uncertainty } fn} \right]}{d + \gamma\, f_2 - \frac{\alpha\,\beta}{(1-\beta\,\kappa)} \left[\underbrace{\frac{1}{(1-\beta\;\Gamma^{d})^2}\,\frac{(\sigma^{d})^2}{2}}_{\text{damage uncertainty}} + \underbrace{\frac{\gamma^2}{(1-\beta\;\Gamma^{fl})^2}\,\frac{(\sigma^{fl})^2}{2}}_{\text{forcing uncertainty } fl} \right]} \right)^{\frac{1}{n}} m_t$$

Social cost of carbon. Inserting (45), (47), (48) and (49) for the shadow values φ_k, $\varphi_{\tau 1}$, φ_π^d, φ_π^{fl} and φ_π^{fn} into our equation for the shadow value of the atmospheric carbon stock (50) and using the definition $\gamma = \beta\,\xi_0\,\tilde{\sigma}$ delivers

$$\begin{aligned}
\varphi_{M1} = -\frac{1}{1-\beta\,\kappa} \Bigg(& \gamma \left(f_1 + f_2\, z^{unc} - f_3\, (z^{unc})^{1-n} \right) + a + d\, z^{unc} \\
& -\alpha\,\beta \Bigg[\underbrace{\frac{1}{(1-\beta\;\Gamma^{d})^2}\,\frac{(\sigma^{d})^2}{2}}_{\text{damage uncertainty}} + \underbrace{\frac{\gamma^2}{(1-\beta\;\Gamma^{fl})^2}\,\frac{(\sigma^{fl})^2}{2}}_{\text{forcing uncertainty } fl} \\
& + \underbrace{\frac{\gamma^{2\,4}}{(1-\beta\;\Gamma^{fn})^2}\,\frac{(\sigma^{fn})^2}{2}(z^{unc})^{-n}}_{\text{forcing uncertainty } fn} \Bigg] z^{unc} \Bigg) M_{pre}^{-1}\,\tilde{\phi}
\end{aligned}$$

The SCC is the negative of the shadow value of the atmospheric carbon stock expressed in money-measured consumption units

$$\begin{aligned}
SCC^{unc} &= -(1-\beta\,\kappa) Y_t^{net}\,\varphi_{M1} \\
&= \frac{Y_t^{net}}{M_{pre}} \Bigg(a + f_1\,\gamma - \left(\frac{f_3}{(z^{unc})^n} - f_2 \right) \gamma z^{unc} + d z^{unc} \\
&\quad -\alpha\,\beta \Bigg[\underbrace{\frac{1}{(1-\beta\;\Gamma^{d})^2}\,\frac{(\sigma^{d})^2}{2}}_{\text{damage uncertainty}} + \underbrace{\frac{\gamma^2}{(1-\beta\;\Gamma^{fl})^2}\,\frac{(\sigma^{fl})^2}{2}}_{\text{forcing uncertainty } fl} \\
&\quad + \underbrace{\frac{\gamma^{2\,4}}{(1-\beta\;\Gamma^{fn})^2}\,\frac{(\sigma^{fn})^2}{2}\frac{1}{(z^{unc})^n}}_{\text{forcing uncertainty } fn} \Bigg] z^{unc} \Bigg) \tilde{\phi}.
\end{aligned}$$

C Climate Change Uncertainty

Dynamic equations. Following Traeger (2018), we model the basic long-run temperature risk resulting from atmospheric carbon dioxide by an autoregressive gamma process y_t, which we shift by a deterministic process y_t^o to adjust temperature expectations. As a result of this base risk, the radiative forcing equation gains the additional contribution

$$\begin{aligned} z_t &\equiv y_t - y_t^o \quad \text{where} \\ y_{t+1}^o &= \gamma^z y_t^o + (\delta_\tau - \epsilon(c, \delta_\tau))(m - \eta_\tau) \end{aligned}$$

is the expectation shifter process and y_t is an autoregressive gamma process Gourieroux and Jasiak (2006) with scale paramter c and shape parameter $\frac{\delta_\tau}{c}(m - \eta_\tau)$. Conditional expectation and variance of the shifted autoregressive gamma process are then

$$\begin{aligned} \mathbb{E}_t\, z_{t+1} &= \underbrace{\gamma^z z_t}_{\substack{\text{shock} \\ \text{persistence}}} + \underbrace{\sigma^{forc} m}_{\text{deterministic forcing}} + \underbrace{\epsilon(c,h)(m - \eta_\tau)}_{\text{expectation offset}} \\ \mathbb{V}\text{ar}_t\, z_{t+1} &= {}^2\,\mathbb{V}\text{ar}_t\, y_{t+1} =^2 c\Big[\underbrace{2\gamma^z y_t}_{\substack{\text{variance} \\ \text{persistence}}} + \underbrace{\delta_\tau (m - \eta_\tau)}_{\substack{\text{base climate} \\ \text{forcing uncertainty}}} \Big]. \end{aligned}$$

The function $\epsilon(c, \delta_\tau)$ is a given function that has to be calibrated together with the scale parameter c and the parameter δ_τ that weighs the current endogenously generated shocks against the persistence of the uncertainty. The parameter $\eta_\tau \in (0, 1)$ calibrates the prevailing uncertainty under (close to) preindustrial concentrations. We refer to a detailed discussion of this formulation of temperature feedback uncertainty to Traeger (2018). The cumulant generating function of the underlying autoregressive gamma process y_t is

$$G_{y_{t+1}}(u) = \log\left[\mathbb{E}\left(\exp(u y_{t+1}) | y_t\right)\right] = -\nu_t \log(1 - uc) + \tfrac{u}{1-uc}\gamma y_t. \tag{53}$$

and will be helpful to evaluate expectations emerging on the r.h.s. of the Bellman equation. The new states y_t and y_t^o will again enter our value function linearly with shadow values φ_y and φ_{y^o}.

In addition, we introduce a stochastic process that captures the uncertainty in the interaction term between carbon dioxide forcing and sulfur-based solar geoengineering. It is of the same form as the process in equation (17) governing sulfur-based forcing

uncertainty

$$\pi_{t+1}^{cn} = \epsilon_t^{cn} \sqrt{\left(\frac{m_t}{S_t}\right)^n S_t} + \Gamma^{cn}\, \pi_t^{cn}. \tag{54}$$

We allow for correlation beetwen the uncertainties governing the interaction of sulfur-based and carbon dioxide-based changes in forcing. As a result the shocks ϵ_t^{cn} and ϵ_t^{fn} have the correlation coefficient ρ^n. The interaction uncertainty introduces the new state π_t^{cn}, which will enter the value function linearly with shadow value φ_π^{cn}.

The full forcing equation takes the form

$$F_t(m_t, S_t) = \frac{\eta}{\log(2)} \log\left(f_0 + f_1\, m_t + \left(f_2 - f_3 \left(\frac{m_t}{S_t}\right)^n\right) S_t + \pi_t^{fl} + \pi_t^{fn} + z_{t+1} + \pi_t^{cn}\right). \tag{55}$$

bringing the equation of motion (27b) for temperature to the form

$$\boldsymbol{\tau}_{t+1} = \boldsymbol{\sigma}\boldsymbol{\tau}_t + \sigma_{\text{forc}}\Big(f_0 + f_1\, m_t + \Big(f_2 - f_3 \Big(\frac{m_t}{S_t^{unc}}\Big)^n\Big) S_t^{unc} + \pi_t^{fl} + \pi_t^{fn} + z_{t+1} + \pi_t^{cn}\Big)\boldsymbol{e}_1. \tag{56}$$

We followed Traeger (2018) in using a slightly different convention for the shifted autoregressive gamma process making $\tau_{1,t+1}$ a function of z_{t+1} (rather than z_t). The additional parameter can be normalized away, but we introduce the parameter explicitly because it allows us to adopt Traeger's (2018) calibration of the process, who works with a different normalization of radiative forcing implying $= \frac{1}{\sigma^{forc}}$.

Changes in the Bellman equation. We first characterize the new terms arising on the r.h.s. of the Bellman equation as a result of the base climate uncertainty. The new stochastic process gives rise to the new equations of motion for the new states y_t^o and y_t, and both of these also show up in the equation of motion of temperature. Using equation (53) we find the the new terms on the r.h.s. Bellman equation where we have set $= \sigma_{forc}$

$$\begin{aligned}
&\frac{\beta}{\alpha}\log\Big(\mathbb{E}_t \exp\left[\alpha\big(\varphi_{\tau,1}(y_{t+1} - y_{t+1}^o) + \varphi_y y_{t+1} + \varphi_{y^o} y_{t+1}^o\big)\right]\Big) \\
&= -\beta\varphi_{\tau,1}\gamma^z y_t^o - \beta\varphi_{\tau,1}(\delta_\tau - \epsilon(c))m_t + \beta\varphi_{\tau,1}(\delta_\tau - \epsilon(c))\big(-\eta_\tau\big) \\
&\quad -\tfrac{\delta_\tau\beta}{\alpha c}(m_t - \eta_\tau)\log(1 - \alpha[\varphi_y^\tau + \varphi_{\tau,1}]c) + \beta\tfrac{\varphi_y^\tau + \varphi_{\tau,1}}{1-\alpha[\varphi_y^\tau+\varphi_{\tau,1}]c}\gamma^z y_t \\
&\quad +\beta\varphi_{y^o}^\tau\gamma^z y_t^o + \beta\varphi_{y^o}^\tau(1 - \epsilon(c))m_t + \beta\varphi_{y^o}^\tau(1 - \epsilon(c))\big(-\eta_\tau\big)
\end{aligned} \tag{57}$$

The interactive uncertainty has the same form as the uncertainty already introduced in

the context of sulfur-based cooling as equation (17). Because we allow for correlation between the uncertainty in equations (17) and equation (54) we have to calculate their expectations jointly and find

$$
\begin{aligned}
&\frac{\beta}{\alpha}\log\left(\mathbb{E}_t\exp\left[\alpha\left(\varphi_\pi^{fn}\pi_{t+1}^{fn}+\varphi_\pi^{cn}\pi_{t+1}^{cn}+\varphi_{\tau,1}\sigma_{forc}(\pi_t^{fn}+\pi_t^{cn})\right)\right]\right)\\
=&\frac{\beta}{\alpha}\log\left(\mathbb{E}_t\exp\left[\alpha\left(\varphi_\pi^{fn}\epsilon_t^{fn}\sqrt{\left(\frac{m_t}{S_t}\right)^n S_t}+\varphi_\pi^{cn}\epsilon_t^{cn}\sqrt{\left(\frac{m_t}{S_t}\right)^n S_t}\right)\right]\right)\\
&\quad+\beta\varphi_\pi^{fn}\Gamma^{fn}\,\pi_t^{fn}+\beta\varphi_\pi^{cn}\Gamma^{cn}\,\pi_t^{cn}+\beta\varphi_{\tau,1}\sigma_{forc}(\pi_t^{fn}+\pi_t^{cn})\\
=&\alpha\,\beta\,(\varphi_\pi^{fn})^2\frac{(\sigma^{fn})^2}{2}\left(\frac{m_t}{S_t}\right)^n S_t+\alpha\,\beta\,\varphi_\pi^{fn}\varphi_\pi^{cn}\rho\sigma^{fn}\sigma^{cn}\left(\frac{m_t}{S_t}\right)^n S_t\\
&\quad+\alpha\,\beta\,(\varphi_\pi^{cn})^2\frac{(\sigma^{cn})^2}{2}\left(\frac{m_t}{S_t}\right)^n S_t\\
&\quad+(\varphi_{\tau 1}\,\sigma_{\text{forc}}+\varphi_\pi^{fn}\,\Gamma^{fn})\beta\;\pi_t^{fn}+(\varphi_{\tau 1}\,\sigma_{\text{forc}}+\varphi_\pi^{cn}\,\Gamma^{cn})\beta\;\pi_t^{cn}\\
=&\alpha\,\beta\left((\varphi_\pi^{fn})^2\frac{(\sigma^{fn})^2}{2}+\varphi_\pi^{fn}\varphi_\pi^{cn}\rho\sigma^{fn}\sigma^{cn}+(\varphi_\pi^{cn})^2\frac{(\sigma^{cn})^2}{2}\right)\left(\frac{m_t}{S_t}\right)^n S_t\\
&\quad+(\varphi_{\tau 1}\,\sigma_{\text{forc}}+\varphi_\pi^{fn}\,\Gamma^{fn})\beta\;\pi_t^{fn}+(\varphi_{\tau 1}\,\sigma_{\text{forc}}+\varphi_\pi^{cn}\,\Gamma^{cn})\beta\;\pi_t^{cn}
\end{aligned}
\tag{58}
$$

Only the first line affects the optimal deployment of sulfur. The second line results in the same coefficient matching condition for π_t^{fn} as before and the exact analogue for π_t^{cn} delivering the shadow values

$$
\varphi_\pi^{fn}=\frac{\varphi_{\tau 1}\,\sigma_{\text{forc}}\,\beta}{1-\beta\;\Gamma^{fn}}=-\frac{\xi_0\,\tilde{\sigma}_{11}\,\sigma_{\text{forc}}\,\beta}{(1-\beta\,\kappa)(1-\beta\;\Gamma^{fn})}\text{ and}
$$

$$
\varphi_\pi^{cn}=\frac{\varphi_{\tau 1}\,\sigma_{\text{forc}}\,\beta}{1-\beta\;\Gamma^{cn}}=-\frac{\xi_0\,\tilde{\sigma}_{11}\,\sigma_{\text{forc}}\,\beta}{(1-\beta\,\kappa)(1-\beta\;\Gamma^{cn})}.
$$

Optimal sulfur deployment. The new terms on the r.h.s. Bellman equation containing sulfur will affect the first order conditions for sulfur deployment. Such terms only arise in the interaction uncertainty stemming from equation (58), not from the base uncertainty. Expanding the definition in equation (42) for the newcomers we have

$$
\begin{aligned}
B_t^S=&\,\beta\,\varphi_{\tau 1}\,\sigma_{\text{forc}}\,f_2\,S_t-\beta\,\varphi_{\tau 1}\,\sigma_{\text{forc}}f_3\,m_t^n\,S_t^{(1-n)}-(1+\beta\,\varphi_k)\,d\,S_t+\alpha\,\beta^{\,2}(\varphi_\pi^d)^2\,\frac{(\sigma^d)^2}{2}\,S_t\\
&+\alpha\,\beta\;(\varphi_\pi^{fl})^2\,\frac{(\sigma^{fl})^2}{2}\,S_t+\alpha\,\beta\,(\varphi_\pi^{fn})^2\frac{(\sigma^{fn})^2}{2}\,m_t^n\,S_t^{(1-n)}\\
&+\alpha\,\beta\left(2\varphi_\pi^{fn}\varphi_\pi^{cn}\rho\sigma^{fn}\sigma^{cn}+(\varphi_\pi^{cn})^2\frac{(\sigma^{cn})^2}{2}\right)m_t^n S_t^{(1-n)}
\end{aligned}
$$

where the last line contains the new terms, which enter the equation for optimal deployment in the same way as the other terms proportional to $m_t^n S_t^{(1-n)}$. Thus, optimizing the above equation w.r.t. sulfur deployment (taking the FOC) delivering the new deployment equation

$$S_t^{joint} = m_t \times \underbrace{\left(\frac{(n-1)\left(\beta\,\varphi_{\tau 1}\,\sigma_{\text{forc}}\,f_3 - \alpha\,\beta\left((\varphi_\pi^{fn})^2\frac{(\sigma^{fn})^2}{2} + 2\varphi_\pi^{fn}\varphi_\pi^{cn}\rho\sigma^{fn}\sigma^{cn} + (\varphi_\pi^{cn})^2\frac{(\sigma^{cn})^2}{2}\right)\right)}{(1+\beta\,\varphi_k)\,d - \beta\,\varphi_{\tau 1}\,\sigma_{\text{forc}} f_2 - \alpha\,\beta^{\,2}(\varphi_\pi^d)^2\frac{(\sigma^d)^2}{2} - \alpha\,\beta\,(\varphi_\pi^{fl})^2\frac{(\sigma^{fl})^2}{2}} \right)^{\frac{1}{n}}}_{\equiv z^{joint}} \tag{59}$$

Inserting the equations for the shadow values and simplifying the resulting expressions delivers

$$S_t^{joint} = m_t \times \left(\frac{(1-n)\,\gamma\,f_3 - \frac{-\alpha\,\beta\,(1-n)}{(1-\beta\,\kappa)}\frac{\gamma^2}{2}\left[\overbrace{\frac{(\sigma^{fn})^2}{(1-\beta\;\Gamma^{fn})^2}}^{\text{geo nonlinear}} + \overbrace{\frac{2\rho\sigma^{fn}\sigma^{cn}}{(1-\beta\;\Gamma^{fn})(1-\beta\;\Gamma^{cn})}}^{\text{correlation geo and clim}} + \overbrace{\frac{(\sigma^{cn})^2}{(1-\beta\;\Gamma^{cn})^2}}^{\text{clim interaction}}\right]}{d + \gamma\,f_2 + \frac{-\alpha\,\beta}{2(1-\beta\,\kappa)}\left[\underbrace{\frac{(\sigma^d)^2}{(1-\beta\;\Gamma^d)^2}}_{\text{damage uncertainty}} + \underbrace{\frac{\gamma^2\;(\sigma^{fl})^2}{(1-\beta\;\Gamma^{fl})^2}}_{\text{geo linear}}\right]} \right)^{\frac{1}{n}}$$

Social cost of carbon. The terms proportional to y_y^o and y_t in equation (57) require the following equality in the Bellman equation (which has to hold for all levels of the state variables):

$$\varphi_{y^o}^\tau y_y^o + \varphi_y^\tau y_t + ... = ... - \beta\varphi_{\tau,1}\gamma^z y_t^o + \beta\frac{\varphi_y^\tau + \varphi_{\tau,1}}{1-\alpha[\varphi_y^\tau+\varphi_{\tau,1}]c}\gamma^z y_t + \beta\varphi_{y^o}^\tau\gamma^z y_t^o$$

Coefficient matching delivers the following equations for the shadow values of the new state variables resulting from basic climate uncertainty

$$\begin{aligned} \varphi_{y^o}^\tau &= \beta(\varphi_{y^o}^\tau - \varphi_{\tau,1})\gamma^z \\ \varphi_y^\tau &= \beta\frac{\varphi_y^\tau+\varphi_{\tau,1}}{1-\alpha c(\varphi_y^\tau+\varphi_{\tau,1})}\gamma^z. \end{aligned} \tag{60}$$

We note that these are currently not yet explicit equation as the prices appear on both sides. In addition, equation (57) delivers the following new terms proportional to the carbon state

$$-\beta\varphi_{\tau,1}(1-\epsilon(c))m_t - \beta\frac{1}{\alpha c}m_t\log(1-\alpha[\varphi_y^\tau+\varphi_{\tau,1}]c) + \beta\varphi_{y^o}^\tau(1-\epsilon(c))m_t$$

and equation (58) delivers the terms

$$\alpha\,\beta\left((\varphi_\pi^{fn})^2\frac{(\sigma^{fn})^2}{2}+2\varphi_\pi^{fn}\varphi_\pi^{cn}\rho\sigma^{fn}\sigma^{cn}+(\varphi_\pi^{cn})^2\frac{(\sigma^{cn})^2}{2}\right)(z^{joint})^{1-n}m_t$$

where the first term in bracket was already present earlier as it results from the nonlinear geoengineering uncertainty. These terms change add to the coefficients in front of the carbon stock in the Bellman equation and change the coefficient matching condition, equation (50), defining the shadow value of carbon to

$$\begin{aligned}\boldsymbol{\varphi}_M^\top=\Bigg(&(\beta\,\varphi_{\tau 1}\,\sigma_{\text{forc}})\left(f_1+f_2\,z-f_3\,z^{1-n}\right)+\alpha\,\beta^{\,2}(\varphi_\pi^d)^2\frac{(\sigma^d)^2}{2}\,z^{joint}+\alpha\,\beta\,(\varphi_\pi^{fl})^2\frac{(\sigma^{fl})^2}{2}\,z^{joint}\\&+\alpha\,\beta\left((\varphi_\pi^{fn})^2\frac{(\sigma^{fn})^2}{2}+\varphi_{2\pi}^{fn}\varphi_\pi^{cn}\rho\sigma^{fn}\sigma^{cn}+(\varphi_\pi^{cn})^2\frac{(\sigma^{cn})^2}{2}\right)(z^{joint})^{1-n}\\&+(\varphi_{y^o}^\tau-\varphi_{\tau,1})(\delta_\tau-\epsilon(c))-\delta_\tau\tfrac{\log(1-\alpha c(\varphi_y^\tau+\varphi_{\tau,1}))}{\alpha c}-(1+\beta\,\varphi_k)(a+d\,z)\Bigg)M_{pre}^{-1}\,\boldsymbol{e}_1^\top\,(\mathbf{1}-\beta\,\boldsymbol{\Phi})^{-1}.\end{aligned}\tag{61}$$

Evaluating the new terms in the last row requires the evaluation of

$$\varphi_{y^o}^\tau-\varphi_{\tau,1}=-\left(\frac{\beta\gamma^z}{1-\beta\gamma^z}+1\right)\varphi_{\tau,1}=-\frac{}{1-\beta\gamma^z}\varphi_{\tau,1}$$

using equation (60) and of

$$\varphi_y^\tau+\varphi_{\tau,1}=\left(1+\theta_\tau^\dagger\right)\frac{}{1-\beta\gamma^z}\varphi_{\tau,1},$$

which solves the quadratic equation (60) delivering the expression

$$\theta_\tau^\dagger=\beta\gamma^z\frac{1+F-\sqrt{(1-F)^2-4F\frac{\beta\gamma^z}{1-\beta\gamma^z}}}{1-F+\sqrt{(1-F)^2-4F\frac{\beta\gamma^z}{1-\beta\gamma^z}}}\approx\frac{\beta\gamma^zF}{1-\beta\gamma^z-F}$$

using the definition $F\equiv\alpha c\frac{}{1-\beta\gamma^z}\varphi_{\tau,1}$. We refer to Traeger (2018) for more details on the

calculation. Then

$$
\begin{aligned}
&(\varphi_{y^o}^{\tau}-\varphi_{\tau,1})(\delta_\tau-\epsilon(c)) - \delta_\tau \tfrac{\log(1-\alpha c(\varphi_y^\tau+\varphi_{\tau,1}))}{\alpha c} \\
&= -\frac{}{1-\beta\gamma^z}\varphi_{\tau,1}(\delta_\tau-\epsilon(c)) - \delta_\tau \tfrac{\log(1-F(1+\theta_\tau^\dagger))}{F}\tfrac{}{1-\beta\gamma^z}\varphi_{\tau,1} \\
&= \frac{}{1-\beta\gamma^z}\varphi_{\tau,1}\Big(\epsilon(c) + \delta_\tau \tfrac{-\log(1-F(1+\theta_\tau^\dagger))}{F} - \delta_\tau\Big) \\
&= -\xi_0\tilde{\sigma}_{1,1}\frac{1}{1-\beta\kappa}\frac{}{1-\beta\gamma^z}\Big(\epsilon(c) + \delta_\tau\Big(\tfrac{-\log(1-F(1+\theta_\tau^\dagger))}{F} - 1\Big)\Big) \\
&= -\frac{\gamma}{\beta}\frac{1}{1-\beta\kappa}\frac{1}{1-\beta\gamma^z}\Big(\epsilon(c) + \underbrace{\delta_\tau\Big(\tfrac{-\log(1-F(1+\theta_\tau^\dagger))}{F} - 1\Big)}_{\equiv\theta(c)}\Big)
\end{aligned}
$$

where, in the last line, we used that we have set $= \sigma_{forc}$ (and the definition $\gamma = \beta\,\xi_0\,\tilde{\sigma}_{1,1}\sigma_{forc}$) and then

$$
\begin{aligned}
F &= \alpha c\frac{\sigma_{forc}}{1-\beta\gamma^z}\varphi_{\tau,1} = -\alpha c\frac{\sigma_{forc}}{1-\beta\gamma^z}\xi_0\tilde{\sigma}_{1,1}\frac{1}{1-\beta\kappa} \\
&= -\alpha c\frac{\gamma}{1-\beta\gamma^z}\frac{1}{1-\beta\kappa}\ .
\end{aligned}
$$

Inserting the shadow values including the expression derived above into equation (61) delivers

$$
\begin{aligned}
\varphi_{M1} = -\frac{1}{1-\beta\,\kappa}\Bigg(&\gamma\left(f_1 + f_2\,z^{joint} - f_3\,(z^{joint})^{1-n}\right) + a + d\,z^{joint} \\
&+\frac{-\alpha\,\beta}{2}\Bigg[\underbrace{\frac{(\sigma^d)^2}{(1-\beta\ \Gamma^d)^2}}_{\text{damage uncertainty}} + \underbrace{\frac{\gamma^2\ (\sigma^{fl})^2}{(1-\beta\ \Gamma^{fl})^2}}_{\text{forcing uncertainty } fl}\Bigg] z^{joint} \\
&+\frac{-\alpha\beta\gamma^2}{2}\Bigg[\underbrace{\frac{(\sigma^{fn})^2}{(1-\beta\ \Gamma^{fn})^2}}_{\text{geo nonlinear}} + \underbrace{\frac{2\rho\sigma^{fn}\sigma^{cn}}{(1-\beta\ \Gamma^{fn})(1-\beta\ \Gamma^{cn})}}_{\text{correlation geo and clim}} + \underbrace{\frac{(\sigma^{cn})^2}{(1-\beta\ \Gamma^{cn})^2}}_{\text{clim interaction}}\Bigg](z^{joint})^{1-n} \\
&+\underbrace{\frac{\gamma}{\beta}\frac{1}{1-\beta\gamma^z}\Big(\epsilon(c) + \underbrace{\tfrac{-\log(1-F(1+\theta_\tau^\dagger(F)))}{F} - 1}_{\equiv\theta^*(F)}\Big)}_{\text{climate change uncertainty } fn}\Bigg) M_{pre}^{-1}\,\tilde{\phi}\ .
\end{aligned}
$$

Translated once again into consumption equivalents we obtain

$$
\begin{aligned}
SCC^{joint} &= -(1-\beta\,\kappa)Y_t^{net}\,\varphi_{M1} \\
&= \frac{Y_t^{net}}{M_{pre}}\Bigg(\gamma\left(f_1+f_2\,z^{joint}-f_3\,(z^{joint})^{1-n}\right)+a+d\,z^{joint} \\
&\quad -\alpha\,\beta\Bigg[\underbrace{\frac{(\sigma^{d})^2}{(1-\beta\;\Gamma^{d})^2}\,\frac{1}{2}}_{\text{damage uncertainty}}+\underbrace{\frac{\gamma^2}{(1-\beta\;\Gamma^{fl})^2}\,\frac{(\sigma^{fl})^2}{2}}_{\text{forcing uncertainty } fl}\Bigg]z^{joint} \\
&\quad -\frac{\alpha\beta\gamma^2}{2}\Bigg[\underbrace{\frac{(\sigma^{fn})^2}{(1-\beta\;\Gamma^{fn})^2}}_{\text{geo nonlinear}}+\underbrace{\frac{2\rho\sigma^{fn}\sigma^{cn}}{(1-\beta\;\Gamma^{fn})(1-\beta\;\Gamma^{cn})}}_{\text{correlation geo and clim}}+\underbrace{\frac{(\sigma^{cn})^2}{(1-\beta\;\Gamma^{cn})^2}}_{\text{clim interaction}}\Bigg](z^{joint})^{1-n} \\
&\quad \underbrace{+\frac{\gamma}{\beta}\frac{1}{1-\beta\gamma^{z}}\Big(\epsilon(c)+\underbrace{\tfrac{-\log(1-F(1+\theta_\tau^{\dagger}(F)))}{F}-1}_{\equiv\theta(F(c))}\Big)\Bigg)\tilde{\phi}}_{\text{climate change uncertainty } fn}\,.
\end{aligned}
$$

D Short-term Uncertainty

The optimization problem in the first period is essentially the one appearing on the right hand side of the Bellman equation (36)

$$
\begin{aligned}
&\max_{x_0,\boldsymbol{N}_0,\boldsymbol{\mathcal{K}}_0,\boldsymbol{E}_0,S_0}\log x_0+\kappa\,k_0+\log\mathcal{F}(\boldsymbol{A}_0,\,\boldsymbol{\mathcal{K}}_0,\,\boldsymbol{N}_0,\,\boldsymbol{E}_0)+\xi_0\;(1-\tau_{1,0})-d\,S_0+\pi_0^{d}-a(m_0-1) \\
&+\frac{\beta}{\alpha}\log\Big(\mathbb{E}_0\exp[\alpha\,\varphi_k\,k_1+\boldsymbol{\varphi}_\tau^{T}\,\boldsymbol{\tau}_1+\boldsymbol{\varphi}_M^{T}\,\boldsymbol{M}_1+\boldsymbol{\varphi}_{R,1}^{T}\,\boldsymbol{R}_1+\varphi_\pi^{d}\,\pi_1^{d}+\varphi_\pi^{fl}\,\pi_1^{fl}+\varphi_\pi^{fn}\,\pi_1^{fn}+\varphi_\pi^{cn}\pi_1^{cn} \\
&+\varphi_1\Big)
\end{aligned}
\tag{62}
$$

with two important differences. First, the parameters d and f_3 are uncertain in the future. Second, conditional on d and f_3 we have already solved for the shadow values characterizing the value of the future states. These two uncertain parameters d and f_3 occur directly in the expressions for next period capital (32) and next period temperature (27b). In addition, both parameters show up directly in the shadow value for carbon and indirectly affect the shadow value of the resource and the affine constant φ_t. Finally, the damage parameter shows up in current period utility, but in the standard timing of dynamic programming current period values are deterministic and, thus, we assume that current period damages take the value d_0 before realizing the true future value. In general,

we pick d_0 to coincide with the expected damage value.

Optimal sulfur deployment. We collected the terms on the r.h.s. of the Bellman equation depending on sulfur deployment in equation (42). In contrast to earlier, now the parameters d and f_3 are uncertain and the equation changes to

$$\begin{aligned} B_0^S = {} & \beta\,\varphi_{\tau 1}\,\sigma_{\text{forc}}\,f_2\,S_0 + \alpha\,\beta^{\,2}(\varphi_\pi^d)^2\,\frac{(\sigma^d)^2}{2}\,S_0 + \alpha\,\beta\,\,(\varphi_\pi^{fl})^2\,\frac{(\sigma^{fl})^2}{2}\,S_0 - d_0\,S_0 \\ & + \alpha\,\beta\,(\varphi_\pi^{fn})^2\frac{(\sigma^{fn})^2}{2}\,m_0^n\,S_0^{(1-n)} + \alpha\,\beta\left(\varphi_\pi^{fn}\varphi_\pi^{cn}\rho\sigma^{fn}\sigma^{cn} + (\varphi_\pi^{cn})^2\frac{(\sigma^{cn})^2}{2}\right)m_0^n S_0^{(1-n)} \\ & + \frac{\beta}{\alpha}\,\log\Big(\,\mathbb{E}_0\exp\Big[\alpha\,\big(-\varphi_{\tau 1}\,\sigma_{\text{forc}} f_3\,m_0^n\,S_0^{(1-n)} - \varphi_k\,d\,S_0\big)\Big]\Big) \end{aligned} \tag{63}$$

where we already evaluated only the (orthogonal) uncertainty governing the evolution of π_t^{fl} and π_t^d (whose terms coincide with equation 42). Defining

$$\begin{aligned} A &\equiv \beta\,\varphi_{\tau 1}\,\sigma_{\text{forc}}\,f_2 + \alpha\,\beta^{\,2}(\varphi_\pi^d)^2\,\frac{(\sigma^d)^2}{2} + \alpha\,\beta\,\,(\varphi_\pi^{fl})^2\,\frac{(\sigma^{fl})^2}{2} - d_0 \\ B &\equiv -\,\varphi_{\tau 1}\,\sigma_{\text{forc}} \\ C &\equiv -\,\varphi_k \\ D &\equiv \alpha\,\beta\left((\varphi_\pi^{fn})^2\frac{(\sigma^{fn})^2}{2} + \varphi_\pi^{fn}\varphi_\pi^{cn}\rho\sigma^{fn}\sigma^{cn} + (\varphi_\pi^{cn})^2\frac{(\sigma^{cn})^2}{2}\right) \end{aligned}$$

we can write equation (63) as

$$B_0^S = A\,S_0 + D\,m_0^n S_0^{(1-n)} + \frac{\beta}{\alpha}\,\log\Big(\,\mathbb{E}_0\exp\Big[\alpha\,\big(B f_3\,m_0^n\,S_0^{(1-n)} + C\,d\,S_0\big)\Big]\Big) \tag{64}$$

Case 1: only f_3 is uncertain and distributed normally. Then $d = d_0$ is deterministic. Letting $f_3 \sim \mathcal{N}(\mu,\,\sigma^2)$, we recall the moment generating function of the normal distribution as $\mathcal{M}(z) = \mathbb{E}_t \exp(z f_3) = \exp(\mu z + \frac{\sigma^2}{2} z^2)$. Then, equation (64) becomes

$$B_0^S = \underbrace{(A + \beta d C)}_{\equiv \bar{A}}\,S_0 + \underbrace{(D\,m_0^n + \beta B m_0^n \mu)}_{\equiv \bar{B}}\,S_0^{1-n} + \underbrace{\beta\alpha B^2 m_0^{2n}\frac{\sigma^2}{2}}_{\equiv \bar{C}}\,S_0^{2-2n} \tag{65}$$

resulting in the first order condition for optimal sulfur deployment

$$\bar{A} + (1-n)\bar{B}\,S_0^{-n} + (2-2n)\bar{C}\,S_0^{1-2n} = 0. \tag{66}$$

Equation (66) implicitly characterizes the optimal control. In order to obtain an analytic form for the expression we approximate the forcing non-linearity as $n = 0.69 \approx \frac{2}{3}$. Then,

the equation becomes

$$\begin{aligned} & \bar{A}\, S_0^n + (1-n)\bar{B} + (2-2n)\bar{C}\, S_0^{1-n} = 0. \\ \Leftrightarrow \quad & \bar{A}\, S_0^{\frac{2}{3}} + (1-n)\bar{B} + (2-2n)\bar{C}\, S_0^{\frac{1}{3}} \;\; = 0. \end{aligned}$$

Letting $y \equiv S_0^{\frac{1}{3}}$, the quadratic equation $\bar{A}x^2 + (2-2n)\bar{C}x + (1-n)\bar{B} = 0$ has the solution

$$\begin{aligned} y \equiv S_0^{\frac{1}{3}} &= \frac{-(2-2n)\bar{C} \pm \sqrt{\left((2-2n)\bar{C}\right)^2 - 4\bar{A}(1-n)\bar{B}}}{2\bar{A}} \\ \Leftrightarrow S_0 &= \left(\frac{-(2-2n)\bar{C} \pm \sqrt{\left((2-2n)\bar{C}\right)^2 - 4\bar{A}(1-n)\bar{B}}}{2\bar{A}} \right)^3 \end{aligned} \tag{67}$$

Using the definitions of $\bar{A}$ and B we can rewrite S_t^{joint} in equation (59) as

$$\left(S_t^{joint}\right)^{\frac{2}{3}} = \left(\frac{(1-n)(\beta\, B\, f_3 + D)}{-\bar{A}} \right) m_t^{\frac{2}{3}} \tag{68}$$

In our stochastic scenario, f_3 is a random variable. In the following, we will use S_t^{joint} to denote equation (68) with f_3 replaced by its expected value μ. Plugging the definitions of $\bar{B}$ and $\bar{C}$ into equation (67) and using (68) in the second step yields

$$\begin{aligned} S_0 &= \left(\frac{-(2-2n)\beta\alpha B^2 m_0^{\frac{4}{3}} \frac{\sigma^2}{2} \pm \sqrt{\left((2-2n)\beta\alpha B^2 m_0^{\frac{4}{3}} \frac{\sigma^2}{2}\right)^2 - 4\bar{A}(1-n)(D\, m_0^{\frac{2}{3}} + \beta B m_0^{\frac{2}{3}} \mu)}}{2\bar{A}} \right)^3 \\ &= \left(\sqrt{(S_0^{joint})^{\frac{2}{3}} + R^2} - R \right)^3 \text{ where } R \equiv \frac{(2-2n)\beta\alpha B^2 m_0^{\frac{4}{3}} \frac{\sigma^2}{2}}{2\bar{A}}. \\ &= \left(\sqrt{(z^{joint})^{\frac{2}{3}} + \bar{R}^2} - \bar{R} \right)^3 m_0 \text{ where } \bar{R} \equiv \frac{(2-2n)\beta\alpha B^2 \frac{\sigma^2}{2}}{2\bar{A}} m_0. \end{aligned} \tag{69}$$

Inserting shadow values. We insert the equations for B and $\bar{A}$ into (69), which leads to

$$\begin{aligned} S_0 &= \left(\sqrt{(S_0^{joint})^{\frac{2}{3}} + R^2} - R \right)^3 \text{ where} \\ R &= \frac{(1-n)\beta\alpha(-\varphi_{\tau 1}\, \sigma_{\text{forc}})^2 m_0^{\frac{4}{3}} \frac{\sigma^2}{2}}{-(1+\beta\,\varphi_k)\, d + \beta\,\varphi_{\tau 1}\,\sigma_{\text{forc}} f_2 + \alpha\,\beta^{\,2} (\varphi_\pi^d)^2 \frac{(\sigma^d)^2}{2} + \alpha\,\beta\,(\varphi_\pi^{fl})^2 \frac{(\sigma^{fl})^2}{2}}. \end{aligned} \tag{70}$$

Inserting (45), (47), (48) and (49) for the shadow values φ_k, $\varphi_{\tau 1}$, φ_π^d and φ_π^{fl} into our expression for optimal sulfur deployment (70) delivers

$$R = \frac{(1-n)\beta\alpha(\frac{\xi_0\,\tilde{\sigma}_{11}\,\sigma_{\text{forc}}}{1-\beta\,\kappa})^2 m_0^{\frac{4}{3}}\frac{\sigma^2}{2}}{-\frac{1}{1-\beta\,\kappa}\,d - \frac{\beta\,\xi_0\,\tilde{\sigma}_{11}\,\sigma_{\text{forc}} f_2}{1-\beta\,\kappa} + \frac{\alpha\,\beta}{(1-\beta\,\kappa)^2}\left[\frac{1}{(1-\beta\,\Gamma^d)^2}\,\frac{(\sigma^d)^2}{2} + \frac{\gamma^2}{(1-\beta\,\Gamma^{fl})^2}\,\frac{(\sigma^{fl})^2}{2}\right]}.$$

Simplifying and using the definition $\gamma = \beta\,\xi_0\,\tilde{\sigma}$ leads to

$$R = \frac{(1-n)\frac{\alpha\,\gamma\,\xi_0\,\tilde{\sigma}}{1-\beta\,\kappa} m_0^{\frac{4}{3}}\frac{\sigma^2}{2}}{-\,d - \gamma\,f_2 + \frac{\alpha\,\beta}{(1-\beta\,\kappa)}\left[\frac{1}{(1-\beta\,\Gamma^d)^2}\,\frac{(\sigma^d)^2}{2} + \frac{\gamma^2}{(1-\beta\,\Gamma^{fl})^2}\,\frac{(\sigma^{fl})^2}{2}\right]} \quad \text{or}$$

$$\bar{R} = \frac{(1-n)\frac{\alpha\,\gamma\,\xi_0\,\tilde{\sigma}}{1-\beta\,\kappa}\frac{\sigma^2}{2}}{-\,d - \gamma\,f_2 + \frac{\alpha\,\beta}{(1-\beta\,\kappa)}\left[\frac{1}{(1-\beta\,\Gamma^d)^2}\,\frac{(\sigma^d)^2}{2} + \frac{\gamma^2}{(1-\beta\,\Gamma^{fl})^2}\,\frac{(\sigma^{fl})^2}{2}\right]}\, m_0\,.$$

We further simplify the formula as follow still using $S_0 = \left(\sqrt{(z^{joint})^{\frac{2}{3}} + \bar{R}^2} - \bar{R}\right)^3 m_0$ with

$$\bar{R} = \frac{-\alpha(1-n)\frac{\gamma^2}{\beta(1-\beta\,\kappa)}}{d + \gamma\,f_2 - \frac{\alpha\,\beta}{(1-\beta\,\kappa)}\left[\frac{1}{(1-\beta\,\Gamma^d)^2}\,\frac{(\sigma^d)^2}{2} + \frac{\gamma^2}{(1-\beta\,\Gamma^{fl})^2}\,\frac{(\sigma^{fl})^2}{2}\right]}\, m_0\,\frac{\sigma^2}{2}\,.$$

$$\bar{R} = \underbrace{\frac{(1-n)\mu\gamma}{d + \gamma\,f_2 - \frac{\alpha\,\beta}{(1-\beta\,\kappa)}\left[\frac{1}{(1-\beta\,\Gamma^d)^2}\,\frac{(\sigma^d)^2}{2} + \frac{\gamma^2}{(1-\beta\,\Gamma^{fl})^2}\,\frac{(\sigma^{fl})^2}{2}\right]}}_{\equiv z^{lin}}\, \frac{-\alpha\gamma}{\beta(1-\beta\,\kappa)}\, m_0\,\frac{\sigma^2}{2\mu}\,.$$

$$\bar{R} = (z^{lin})^{\frac{2}{3}}\, \underbrace{\frac{-\alpha\gamma}{\beta(1-\beta\,\kappa)}\, m_0\,\frac{\sigma^2}{2\mu}}_{\equiv x^{old}}\,.$$

where z^{lin} is the geoengineering propensity in the absence of non-linear uncertainty, i.e., the uncertainty governed by equations (17) and (54).

$$
\begin{aligned}
S_0 &= \left(\sqrt{(z^{joint})^{\frac{2}{3}} + \left((z^{lin})^{\frac{2}{3}} x \right)^2} - (z^{lin})^{\frac{2}{3}} x \right)^3 m_0 \\
&= z^{joint} \left(\sqrt{1 + \left(\frac{(z^{lin})^2}{z^{joint}} \right)^{\frac{1}{3}} x^2} - \left(\frac{(z^{lin})^2}{z^{joint}} \right)^{\frac{1}{3}} x \right)^3 m_0 \\
&= z^{lin} \left(\sqrt{\left(\frac{z^{joint}}{z^{lin}} \right)^{\frac{2}{3}} + \left((z^{lin})^{\frac{1}{3}} x \right)^2} - (z^{lin})^{\frac{1}{3}} x \right)^3 m_0 \quad \text{with} \\
x &= \frac{\bar{R}}{(z^{lin})^{\frac{2}{3}}} = \underbrace{\frac{-\alpha\gamma}{\beta(1-\beta\,\kappa)}\, m_0 \frac{\sigma^2}{2\mu}}_{\equiv x} .
\end{aligned}
$$

The version stated in the main text defines $Q = \left(\frac{(z^{lin})^2}{z^{joint}} \right)^{\frac{1}{3}} x$ and uses the formulation in the second line above. We note that without the nonlinear interaction uncertainty we have the slightly simpler formula:

$$
\begin{aligned}
S_0 &= \left(\sqrt{(z^{unc})^{\frac{2}{3}} (1 + (z^{unc})^{\frac{2}{3}} x^2)} - (z^{unc})^{\frac{2}{3}} x \right)^3 m_0 \\
&= \left((z^{unc})^{\frac{1}{3}} \sqrt{1 + (z^{unc})^{\frac{2}{3}} x^2} - (z^{unc})^{\frac{2}{3}} x \right)^3 m_0 \\
&= z^{unc} \left(\sqrt{1 + (z^{unc})^{\frac{2}{3}} x^2} - (z^{unc})^{\frac{1}{3}} x \right)^3 m_0
\end{aligned}
$$

For our presentation in the main text we would then have $Q = (z^{unc})^{\frac{1}{3}} x$.

Social Cost of Carbon. The shadow value of atmospheric carbon depends directly and non-linearly on f_2. As a result, we have to evaluate the expectations in equation (62) numerically.

Case 2: only f_3 is uncertain and Gamma distributed. Let $f_3 \sim \Gamma(\bar{k}, \theta)$ with shape parameter $\bar{k}$ and a scale parameter θ. Then, the moment generating function is $\mathcal{M}(z) = \mathbb{E}_t \exp(z f_3) = (1 - \theta z)^{-\bar{k}}$, where we assume $z < \frac{1}{\theta}$. Equation (63) becomes

$$
B_0^S = \underbrace{(A + d\beta C)}_{\equiv \bar{A}} S_0 + D\, m_0^n S_0^{(1-n)} - \frac{\beta}{\alpha} \bar{k} \log \left(1 - \theta \alpha B m_0^n\, S_0^{1-n} \right)
$$

resulting in the first order condition for optimal sulfur deployment

$$\bar{A}+(1-n)D\,m_0^n S_0^{-n}+(1-n)\frac{\beta}{\alpha}\bar{k}\frac{\theta\alpha B m_0^n\,S_0^{-n}}{1-\theta\alpha B m_0^n\,S_0^{1-n}}=0$$

$$\Leftrightarrow \bar{A}\left(1-\theta\alpha B m_0^n\,S_0^{1-n}\right)+(1-n)D\,m_0^n S_0^{-n}\left(1-\theta\alpha B m_0^n\,S_0^{1-n}\right)+(1-n)\frac{\beta}{\alpha}\bar{k}\theta\alpha B m_0^n\,S_0^{-n}=0$$

$$\Leftrightarrow \bar{A}-\bar{A}\theta\alpha B m_0^n\,S_0^{1-n}+(1-n)Dm_0^n\,S_0^{-n}-(1-n)D\,m_0^{2n}S_0^{1-2n}\theta\alpha B+(1-n)\frac{\beta}{\alpha}\bar{k}\theta\alpha B m_0^n\,S_0^{-n}=0$$

$$\Leftrightarrow \bar{A}S_0^n-\bar{A}\theta\alpha B m_0^n\,S_0+(1-n)Dm_0^n-(1-n)D\,m_0^{2n}S_0^{1-n}\theta\alpha B+(1-n)\frac{\beta}{\alpha}\bar{k}\theta\alpha B m_0^n=0$$

$$\Leftrightarrow \bar{A}S_0^n-\bar{A}\theta\alpha B m_0^n\,S_0-(1-n)D\,\theta\alpha B m_0^{2n}S_0^{1-n}+(1-n)\left(\frac{\beta}{\alpha}\bar{k}\theta\alpha B+D\right)m_0^n=0$$

$$\Leftrightarrow \bar{A}S_0^n+\underbrace{\left(-\bar{A}\theta\alpha B m_0^n\right)}_{\equiv\bar{B}}S_0+\Big(-(1-n)D\,\theta\alpha B m_0^{2n}\Big)S_0^{1-n}+\underbrace{(1-n)\left(\beta\bar{k}\theta B+D\right)m_0^n}_{\equiv\bar{C}}=0$$

D.1 Joint Gamma Uncertainty

In this setting, we introduce uncertainty already at the onset of the period. Otherwise, we would have to assume that damages during the first period are known. As a result, the Bellman equation becomes

$$\max_{x_1,\boldsymbol{N}_1,\boldsymbol{\mathcal{K}}_1,\boldsymbol{E}_1,S_1}\frac{1}{\alpha}\log\Big(\mathbb{E}_0\exp\big[\alpha\Big(\tag{71}$$

$$\log x_1+\kappa\,k_1+\log\mathcal{F}(\boldsymbol{A}_1,\,\boldsymbol{\mathcal{K}}_1,\,\boldsymbol{N}_1,\,\boldsymbol{E}_1)+\xi_1\,(1-\tau_{1,1})-d\,S_1+\pi_1^d-a(m_1-1)$$

$$+\frac{\beta}{\alpha}\log\Big(\mathbb{E}_1\exp\left[\alpha\left(\varphi_k\,k_2+\boldsymbol{\varphi}_\tau^T\,\boldsymbol{\tau}_2+\boldsymbol{\varphi}_M^T\,\boldsymbol{M}_2+\boldsymbol{\varphi}_{R,2}^T\,\boldsymbol{R}_2+\varphi_d\,\pi_2^d+\varphi_f\,\pi_2^{fl}+\varphi_2\right)\right]\Big)\big]\Big)\Big)$$

We note that $\frac{1}{\alpha}\log$ could be eliminated up to the sign (they are but a strictly monotonic transformation); we keep them as they simplify the resulting expressions.

We assume that sulfur's forcing uncertainty is governed by $f_3\sim\Gamma(\bar{k}^{fl},\theta^{fl})$ with shape parameter $\bar{k}^{fl}$ and a scale parameter θ^{fl}. We assume that geoengineering damages are distributed $d\sim\Gamma(\bar{k}^d,\theta^d)$ with shape parameter $\bar{k}^d$ and a scale parameter θ^d. We assume that both random variables are independently distributed. The moment generating function of the gamma distribution is $\mathcal{M}(z)=\mathbb{E}_t\exp(zf_3)=(1-\theta z)^{-\bar{k}}$, where we assume $z<\frac{1}{\theta}$.

In evaluating equation (71), we assume that the first instance of long-term uncertainty resolves in period 1 and, thus, is governed by the expected value operator $\mathbb{E}_1$ at the end of period 1 (or the beginning of period 2). The short-term uncertainty, i.e., our gamma

distributed parameters d and f_3, are governed by the immediate uncertainty evaluated by $\mathbb{E}_0$. Collecting again only terms depending on S_0, equation (63) becomes

$$
\begin{aligned}
B_0^S = \frac{1}{\alpha}\,\log\Big(\,\mathbb{E}_0\exp\Big[\alpha\,\big(\beta\,\varphi_{\tau 1}\,\sigma_{\text{forc}}\,f_2\,S_0 \\
&+\alpha\,\beta^{\,2}(\varphi_\pi^d)^2\,\frac{(\sigma^d)^2}{2}\,S_0+\alpha\,\beta\,(\varphi_\pi^{fl})^2\,\frac{(\sigma^{fl})^2}{2}\,S_0-d\,S_0 \\
&+\alpha\,\beta\left((\varphi_\pi^{fn})^2\frac{(\sigma^{fn})^2}{2}+\varphi_\pi^{fn}\varphi_\pi^{cn}\rho\sigma^{fn}\sigma^{cn}+(\varphi_\pi^{cn})^2\frac{(\sigma^{cn})^2}{2}\right)m_0^n S_0^{(1-n)} \\
&-\beta\varphi_{\tau 1}\,\sigma_{\text{forc}}f_3\,m_0^n\,S_0^{(1-n)}-\beta\varphi_k\,d\,S_0\big)\Big]\Big) \\
=\underbrace{\beta\,\varphi_{\tau 1}\,\sigma_{\text{forc}}\,f_2\,S_0+\alpha\,\beta^{\,2}(\varphi_\pi^d)^2\,\frac{(\sigma^d)^2}{2}\,S_0+\alpha\,\beta\,(\varphi_\pi^{fl})^2\,\frac{(\sigma^{fl})^2}{2}}_{\equiv A}\,S_0 \\
+\underbrace{\alpha\,\beta\left((\varphi_\pi^{fn})^2\frac{(\sigma^{fn})^2}{2}+\varphi_\pi^{fn}\varphi_\pi^{cn}\rho\sigma^{fn}\sigma^{cn}+(\varphi_\pi^{cn})^2\frac{(\sigma^{cn})^2}{2}\right)m_0^n}_{\equiv G}\,S_0^{(1-n)} \\
+\frac{1}{\alpha}\,\log\Big(\,\mathbb{E}_0\exp\Big[\alpha\,\big(-\beta\varphi_{\tau 1}\,\sigma_{\text{forc}}f_3\,m_0^n\,S_0^{(1-n)}-(1+\beta\varphi_k)d\,S_0\big)\Big]\Big) \\
= AS_0+GS_0^{(1-n)}-\frac{\bar{k}^{fl}}{\alpha}\log\big(1+\theta^{fl}\beta\alpha\varphi_{\tau 1}\,\sigma_{\text{forc}}\,m_0^n\,S_0^{1-n}\big)-\frac{\bar{k}^d}{\alpha}\log\big(1+\theta^d\alpha(1+\beta\varphi_k)S_0\big) \qquad (72)
\end{aligned}
$$

Equation (72) delivers the first order condition for optimal sulfur deployment

$$
A-\frac{\bar{k}^{fl}}{\alpha}\frac{(1-n)\theta^{fl}\beta\alpha\varphi_{\tau 1}\,\sigma_{\text{forc}}\,m_0^n\,S_0^{-n}}{1+\theta^{fl}\beta\alpha\varphi_{\tau 1}\,\sigma_{\text{forc}}\,m_0^n\,S_0^{1-n}}-\frac{\bar{k}^d}{\alpha}\frac{\theta^d\alpha(1+\beta\varphi_k)}{1+\theta^d\alpha(1+\beta\varphi_k)\,S_0}=0.
$$

Defining as well (note: A, B, C differ here sligthtly from above definitions)

$$
B\equiv\alpha\beta\,\varphi_{\tau 1}\,\sigma_{\text{forc}}
$$

$$
C\equiv\alpha(1+\beta\,\varphi_k)
$$

the equation can be rewritten as

$$
A+(1-n)GS_0^{-n}-\frac{\bar{k}^{fl}}{\alpha}\frac{(1-n)\theta^{fl}B\,m_0^n\,S_0^{-n}}{1+\theta^{fl}B\,m_0^n\,S_0^{1-n}}-\frac{\bar{k}^d}{\alpha}\frac{\theta^dC}{1+\theta^dC\,S_0}=0. \qquad (73)
$$

We solve equation (73) numerically. The mean of the Gamma distribution is $\mu=k\theta$, the variance is $\sigma^2=k\theta^2$. We determine shape parameters using our deterministic best-guess-values for μ and picking σ. Observing that $\sigma^2=k\theta^2=\mu\theta$ we then obtain the scale and

shape parameters as

$$\theta^i = \frac{\sigma_i^2}{\mu_i} \quad \text{and} \quad k^i = \frac{\mu_i}{\theta^i} \quad \text{for } i \in \{f, d\}.$$

If we replace the gamma distribution over f_3 with a normal distribution, then we simply replace the corresponding gamma term above with the normal version from equation (65) and find the implicit equation

$$\begin{aligned} A + (1-n) G S_0^{-n} - \frac{\bar{k}^{fl}}{\alpha} \frac{(1-n)\theta^{fl} B\, m_0^n\, S_0^{-n}}{1 + \theta^{fl} B\, m_0^n\, S_0^{1-n}} - \varphi_{\tau 1}\, \sigma_{\text{forc}} \beta m_0^n \mu\, S_0^{1-n} \\ + \alpha (\varphi_{\tau 1})^2 \, (\sigma_{\text{forc}})^2 \beta^2 m_0^{2n} \frac{\sigma^2}{2}\, S_0^{2-2n} \quad = \quad 0. \end{aligned}$$